Cofacial Assembly of Partially Oxidized Metallomacrocycles as an Approach To Controlling Lattice Architecture in Low-Dimensional Molecular "Metals". Probing Band Structure–Counterion Interactions in Conductive [M(phthalocyaninato)O]$_n$ Macromolecules Using Nitrosonium Oxidants

Tamotsu Inabe,[1a] John G. Gaudiello,[1a] Michael K. Moguel,[1a] Joseph W. Lyding,[1b] Robert L. Burton,[1b] William J. McCarthy,[1b] Carl R. Kannewurf,[1b] and Tobin J. Marks*[1a]

Contribution from the Department of Chemistry, the Department of Electrical Engineering and Computer Science, and the Materials Research Center, Northwestern University, Evanston, Illinois 60201. *Received June 2, 1986*

Abstract: This contribution reports an integrated chemical and physicochemical investigation of the consequences of doping the cofacially joined metallomacrocyclic polymers [M(Pc)O]$_n$, M = Si and Ge, with the nitrosonium salts NO^+X^-, $X^- = BF_4^-$, PF_6^-, and SbF_6^-. In the case of [Si(Pc)O]$_n$, doped products $\{[Si(Pc)O]X_y\}_n$ are obtained with a limiting stoichiometry $y \approx 0.36$ (essentially identical with band-fillings obtained with halogen oxidants). In contrast, NO^+X^- doping results in decomposition of [Ge(Pc)O]$_n$. Upon incremental NO^+X^- doping of [Si(Pc)O]$_n$, transmission infrared spectra reveal the progressive growth of electronic absorption, and transmission optical spectra reveal the formation of Pc π radical cation species. Studies of the NO^+X^- doping process by X-ray diffractometry suggest that it is largely inhomogeneous. Computer-assisted analysis of the $\{[Si(Pc)O]X_y\}_n$ powder diffraction data (aided by judiciously chosen model compounds) indicates crystal structures closely analogous to those of $\{[Si(Pc)O](I_3)_{0.37}\}_n$, $\{[Si(Pc)O](Br_3)_{0.37}\}_n$, $Ni(Pc)(ClO_4)_{0.40}$, and $Ni(Pc)(BF_4)_{0.35}$. The data can be indexed in the tetragonal space group $P4/mcc$, $Z = 2$, with $a = 13.70$ (7) Å, $c = 6.58$ (4) Å, phthalocyanine staggering angle = 40 (2)° ($X^- = BF_4^-$); $a = 13.98$ (6) Å, $c = 6.58$ (4) Å; phthalocyanine staggering angle = 40 (2)° ($X^- = PF_6^-$); $a = 14.31$ (4) Å, $c = 6.58$ (4) Å, phthalocyanine staggering angle = 40 (2)° ($X^- = SbF_6^-$). It appears that the X^- ions are disordered along c. ESR spectra reveal nearly free electron g values, in accord with the ligand-centered π radical character of the oxidation. As a consequence of the pronounced unidimensionality and minimal interaction of the carriers with heavy atoms, X-band powder ESR line widths are rather narrow (2.9–0.36 G) and decrease in the order $I_3^- > SbF_6^- > PF_6^- > BF_4^-$. For $\{[Si(Pc)O](BF_4)_{0.36}\}_n$, the line width is virtually temperature-independent from 4 to 300 K. Variable temperature (4–300 K) static magnetic susceptibility studies of the $\{[Si(Pc)O]X_y\}_n$ materials reveal a small, sample-dependent Curie-like component and a Pauli-like, weakly temperature dependent contribution. Within experimental error, the Pauli-like susceptibility is independent of X^-. Optical reflectivity studies of these materials reveal a plasma edge in the infrared. A Drude analysis of the data yields plasma frequency and tight-binding bandwidth parameters which are essentially independent of X^-. Four-probe electrical conductivity studies of polycrystalline $\{[Si(Pc)O]X_y\}_n$ samples reveal a sharp increase of conductivity with increasing y. The temperature dependence of the data can be most convincingly fit to a transport model involving fluctuation-induced carrier tunneling through parabolic potential barriers that separate the high conductivity regions. As for the other collective properties, the charge transport properties are relatively insensitive to X^-. A thermochemical analysis (Born–Haber cycle) indicates that the energetics of [Si(Pc)O]$_n$ doping with Br_2, I_2, and NO^+X^- are surprisingly similar. The small magnitude of the band structure–counterion interactions in the $\{[Si(Pc)O]X_y\}_n$ materials is attributed both to the local electronic and molecular structure of the phthalocyanine subunits as well as the overall stacking rigidity imposed by the $-(Si-O-)_n$ chains.

The structural, optical, magnetic, and charge transport characteristics of low-dimensional molecular "metals"[2] are a sensitive function of various electrostatic and covalent interactions that occur between the molecular array forming the band structure and charge-compensating off-axis counterions (e.g., the partially oxidized multimolecular assembly in A). The nature and magnitudes of these interactions doubtless have a crucial influence

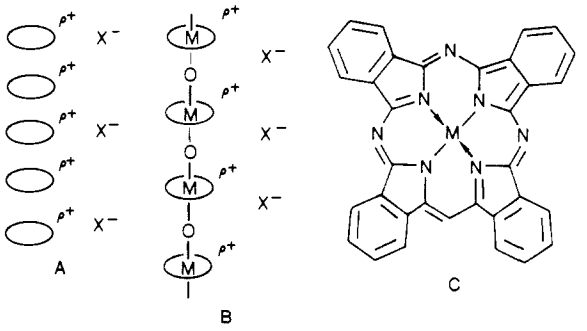

on stacking architecture (including the absence of stacking),[2,3] the degree of band filling (ρ) that can ultimately be achieved,[2-4]

(1) (a) Department of Chemistry. (b) Department of Electrical Engineering and Computer Science.

(2) (a) *Proceedings of the International Conference on the Physics and Chemistry of Low-Dimensional Synthetic Metals (ICSM 84)*; Pecile, C.; Zerbi, G.; Bozio, R.; Girlando, A., Eds.; Abano Terme, Italy, June 17–22, 1984. *Mol. Cryst. Liq. Cryst.* **1985**, *117–121*. (b) Williams, J. M. *Prog. Inorg. Chem.* **1985**, *33*, 183–220. (c) Wudl, F. *Acc. Chem. Res.* **1984**, *17*, 227–232. (d) Greene, R. L.; Street, G. B. *Science (Washington, DC)* **1984**, *226*, 651–656. (e) *Extended Linear Chain Compounds*; Miller, J. S., Ed.; Plenum Press: New York, 1982; Vols. 1, 2, and 3. (f) *Proceedings of the International Conference on Low-Dimensional Conductors*; Epstein, A. J.; Conwell, E. M., Eds.; Boulder, Colorado, August 9–14, 1981. *Mol. Cryst. Liq. Cryst.* **1981–1982**, *77*, *79*, *81*, *83*, *85*, *86*, Parts A–F. (g) Jérome, D.; Schulz, H. J. *Adv. Phys.* **1982**, *31*, 299–490. (h) *The Physics and Chemistry of Low-Dimensional Solids*; Alcacer, L., Ed.; D. Reidel: Dordrecht, 1980. (i) *Highly Conducting One-Dimensional Solids*; Devreese, J. T.; Evrard, R. P.; van Doren, V. E., Eds.; Plenum Press: New York, 1979.

(3) (a) Marks, T. J.; Kalina, D. W. In ref 2e, Vol. 1, pp 197–331. (b) Delhaes, P. *Mol. Cryst. Liq. Cryst.* **1983**, *96*, 229–262. (c) Torrance, J. B. *Acc. Chem. Res.* **1979**, *12*, 79–86.

(4) (a) Wiygul, F. M.; Metzger, R. M.; Kistenmacher, T. J. *Mol. Cryst. Liq. Cryst.* **1984**, *107*, 115–131, and references therein. (b) Metzger, R. M. *J. Chem. Phys.* **1981**, *75*, 3087–3096. (c) Torrance, J. B.; Silverman, B. D. *Phys. Rev. B* **1977**, *15*, 788–801. (d) Epstein, A. J.; Lipari, N. O.; Sandman, D. J.; Nielson, P. *Phys. Rev. B* **1976**, *13*, 1569–1579.

0002-7863/86/1508-7595$01.50/0

Coulombic screening effects,[4,5] and the onset of both charge and spin density wave as well as superconducting phenomena.[2,6] In clarifying the nature of these interactions, it would be highly desirable to have available for comparison a molecular based band structure system in which the connectivity of the molecular stacking architecture was rigorously enforced. This would help to differentiate among those effects arising directly from stack structural perturbations vs. various types of less direct carrier–counterion interactions (electrostatic, phonon, etc.).

The linking of metallomacrocycles into cofacial arrays (e.g., B) represents an effective approach to constraining stacking architecture in metallomacrocyclic conductors.[3a,7,8] In the case of the phthalocyanine (C, Pc) macrocycle, M = Si, Ge, we have reported in detail on the chemical structural, magnetic, optical, and electrical properties of the materials prepared with halogen dopants (B, $X^- = Br_3^-, I_3^-$, $\rho \sim +0.35$),[7] Comparison of these properties with those of $[M(Pc)O]_n$ materials prepared with very different oxidizing agents and containing very different X^- counterions should be highly informative.[3,9] In the present contribution, we describe such an investigation, employing the nitrosonium ion as an oxidizing agent (eq 1)[10] and introducing,

$$[M(Pc)O]_n + yNO^+X^- \rightarrow \{[M(Pc)O]X_y\}_n + yNO(g) \quad (1)$$

$$M = Si, Ge; X^- = BF_4^-, PF_6^-, SbF_6^-$$

sequentially, counterions of appreciably different size, shape, and polarizability than the trihalides. This study represents, to our knowledge, the first case in which a substitution as drastic as $I_3^- \rightarrow BF_4^-, PF_6^-, SbF_6^-$ has been achieved for a molecular conductor without major structural reorganization occurring in the molecular stack.[2,3] This study also represents the first detailed investigation of a metallomacrocyclic conductor with a counterion other than trihalide.[11] It will be seen that the band structure–counterion interactions in this case are surprising for a molecular "metal" and that they can be understood largely on the basis of the distinctive crystal and electronic structures involved. We also present a thermochemical analysis of the cohesive energies involved in doping a phthalocyanine with nitrosonium salts vis-à-vis iodine and bromine.

Experimental Section

Materials. The polymer $[Si(Pc)O]_n$ was prepared as described previously with vacuum sublimed (400 °C/10^{-5} torr) $Si(Pc)Cl_2$ as the starting material.[7d] The average degree of polymerization ($\bar{n}$) was greater than 100. The polymer $[Ge(Pc)O]_n$, $\bar{n} \geq 70$, was also prepared by the literature procedure.[7d] The doping agent $NO^+BF_4^-$ (Alfa) was purified by vacuum sublimation at 200 °C, while $NO^+PF_6^-$ and $NO^+SbF_6^-$ (Alfa, packaged under argon) were used without further purification. The nitrosonium reagents were stored and handled at all times with strict exclusion of moisture and oxygen (Schlenk ware or a Vacuum Atmospheres glovebox with an efficient recirculator). The purity of these reagents was routinely checked by infrared spectroscopy. Methylene chloride was purified by distillation from P_2O_5 under nitrogen. Other solvents were dried in a manner appropriate to each.

Elemental analyses to determine doping levels were performed by Galbraith Microanalytical Laboratories.

Synthesis of $\{[Si(Pc)O]X_y\}_n$ Compounds. In the glovebox, finely ground $[Si(Pc)O]_n$ and the desired amount of $NO^+BF_4^-$, $NO^+PF_6^-$, or $NO^+SbF_6^-$ were weighed into a Schlenk tube. A stirring bar was added, and the vessel was closed and removed from the glovebox. On a vacuum line, dry CH_2Cl_2 was freeze–thaw degassed and condensed into the reaction vessel (ca. 10 mL/0.10 g polymer). Under a slow flush of prepurified N_2, the reaction mixture was then vigorously stirred for 6–12 h at room temperature. Neither longer reaction times nor very large excesses of the nitrosyl salt affected the limiting stoichiometry which could be achieved (vide infra). At the completion of the reaction, the product was isolated by filtration under nitrogen or centrifugation. It was then washed sequentially with 3 × 20 mL of dry CH_2Cl_2, followed by methanol, acetone, and ether. Finally, the doped polymers were dried under high vacuum for 14–20 h to yield dark, air-stable, microcrystalline powders.

Attempted Doping of $[Ge(Pc)O]_n$. The procedure described above was carried out with $[Ge(Pc)O]_n$ and various of the NOX salts in CH_2Cl_2. Workup yielded products which did not exhibit the characteristic electronic absorption of partially oxidized $[Ge(Pc^{\rho+})O]_n$[7c] in the infrared. Rather, marked diminution of the locally antisymmetric Ge–O–Ge stretching mode at 865 cm^{-1} [7d] was observed as well as the appearance of a number of new spectral transitions.

Transmission Infrared Spectroscopy. Transmission infrared spectra of doped polymers were recorded as KBr pellets or as Nujol mulls between KBr plates, by using Perkin-Elmer Model 283 or 599-B spectrometers, and were calibrated with polystyrene film. Multiple scans were performed to check for possible decomposition.

Transmission Optical Spectroscopy. Transmission optical spectra were recorded on Nujol mulls between quartz plates with a Perkin-Elmer Model 330 spectrophotometer. Several scans were routinely made to verify that no decomposition was occurring.

X-ray Diffraction. X-ray powder diffractometry was carried out with a Rigaku Geigerflex instrument with Ni-filtered Cu Kα radiation and the sampling/calibration techniques described previously.[7c,d] To avoid preferential crystallite orientation upon pressing sample pellets, a number of specimens were also studied as unpressed powders by supporting the samples on glass plates covered with a light coating of silicone grease. Computer simulation of diffraction data was carried out as described previously.[7c,d] Densities were measured by aqueous $ZnCl_2$ flotation techniques.[12a]

ESR Spectroscopy. Electron spin resonance experiments were carried out on a modified Varian E-4 X-band ESR spectrometer equipped with a 9 in. magnet and by using 100-kHz field modulation. The field was calibrated with 2,2-phenyl-1-picrylhydrazyl (DPPH, $g = 2.0036$). The cavity resonance frequency was measured to an accuracy of 5 ppm by a transfer oscillator technique. Spin susceptibilities were measured by numerically integrating the first derivative spectra twice with a Fabritek 1074 computer. To reduce any error arising from a variation of the spectrometer sensitivity with temperature and to allow comparison with static susceptibility data (vide infra), absolute ESR-derived spin concentrations were calculated by comparing the integrated intensities of the sample with that of a known amount of DPPH (spins/molecule = 0.99 at higher temperatures, 0.47 at lower temperatures by the Faraday balance technique[12b]) at the same temperature diluted in KBr. Temperatures above 77 K were obtained by use of a conventional quartz dewar employing liquid nitrogen and an electrical heater. Temperatures below 77 K were achieved with an Air Products LTD-3 Helitran. Samples were prepared by sealing known amounts of powdered samples in 1-mm quartz tubes. Sample lengths were sufficient to completely span

(5) (a) Miller, J. S.; Epstein, A. J. *Science (Washington, DC)*, in press. (b) Epstein, A. J.; Miller, J. S.; Pouget, J. P.; Comès, R. *Phys. Rev. Lett.* **1981**, *47*, 741–744. (c) Gutfreund, H.; Little, W. A. In ref 2e, pp 305–372.

(6) (a) Bechgaard, K.; Jérome, D. *Sci. Am.* **1982**, *247*, 52–61. (b) Williams, J. M.; Beno, M. A.; Sullivan, J. C.; Banovetz, L. M.; Braam, J. M.; Blackman, G. S.; Carlson, C. D.; Greer, D. L.; Loesing, D. M. *J. Am. Chem. Soc.* **1983**, *105*, 643–645. (c) Whangbo, M.-H.; Williams, J. M.; Beno, M. A.; Dorfman, J. R. *J. Am. Chem. Soc.* **1983**, *105*, 646–648. (d) Williams, J. M. *Prog. Inorg. Chem.* **1985**, *33*, 183–220.

(7) (a) Marks, T. J. *Science (Washington, DC)* **1985**, *227*, 881–889. (b) Dirk, C. W.; Marks, T. J. *Inorg. Chem.* **1984**, *23*, 4325–4332. (c) Diel, B. N.; Inabe, T.; Lyding, J. W.; Schoch, K. F., Jr.; Kannewurf, C. R.; Marks, T. J. *J. Am. Chem. Soc.* **1983**, *105*, 1551–1567. (d) Dirk, C. W.; Inabe, T.; Schoch, K. F., Jr.; Marks, T. J. *J. Am. Chem. Soc.* **1983**, *105*, 1539–1550. (e) Dirk, C. W.; Inabe, T.; Lyding, J. W.; Schoch, K. F., Jr.; Kannewurf, C. R.; Marks, T. J. *J. Polym. Sci., Polym. Symp.* **1983**, *70*, 1–29. (f) Dirk, C. W.; Mintz, E. A.; Schoch, K. F., Jr.; Marks, T. J. *J. Macromol. Sci.-Chem.* **1981**, *A16*, 275–298.

(8) For studies of isoelectronic Group IIIA $[M(Pc)F]_n$ materials, see: (a) Nohr, R. S.; Kuznesof, P. M.; Wynne, K. J.; Kenney, M. E.; Siebenman, P. G. *J. Am. Chem. Soc.* **1981**, *103*, 4371–4377. For studies of $[M(Pc)L]_n$ materials where L is a bridging organic ligand and M is a transition metal, see: (b) Hanack, M. *Mol. Cryst. Liq. Cryst.* **1984**, *105*, 133–149. (c) Diel, B. N.; Inabe, T.; Jaggi, N.; Lyding, J. W.; Schneider, O.; Hanack, M.; Kannewurf, C. R.; Marks, T. J.; Schwartz, L. J. *J. Am. Chem. Soc.* **1984**, *106*, 3207–3214. (d) Hanack, M. *Chimia* **1983**, *37*, 238–247.

(9) Marks, T. J.; Dirk, C. W.; Schoch, K. F., Jr.; Lyding, J. W. In *Molecular Electronic Devices*; Carter, F. L., Ed.; Marcel Dekker: New York, 1982; pp 195–210.

(10) (a) Weber, D. C.; Brant, P.; Nohr, R. S.; Haupt, S. G.; Wynne, K. J. *J. Phys. (Paris)* **1983**, *C3*, 639–644. (b) Inabe, T.; Lyding, J. W.; Moguel, M. K.; Kannewurf, C. R.; Marks, T. J. *Mol. Cryst. Liq. Cryst.* **1983**, *93*, 355–367. (c) Inabe, T.; Nakamura, S.; Liang, W.-B.; Marks, T. J.; Burton, R. L.; Kannewurf, C. R.; Imaeda, K. I. *J. Am. Chem. Soc.* **1985**, *107*, 7224–7226.

(11) (a) Preliminary accounts of this work and studies with molecular phthalocyanines are given in ref 10b and c. (b) Inabe, T.; Nakamura, S.; Liang, W.-B.; McCarthy, W. J.; Kannewurf, C. R.; Imaeda, K.-I.; Marks, T. J., submitted for publication.

(12) (a) Tadokaro, H. *Structure of Crystalline Polymers*; Wiley-Interscience: New York, 1979; pp 82–83. (b) Duffy, W.; Standburg, D. L. *J. Chem. Phys.* **1967**, *46*, 456–464.

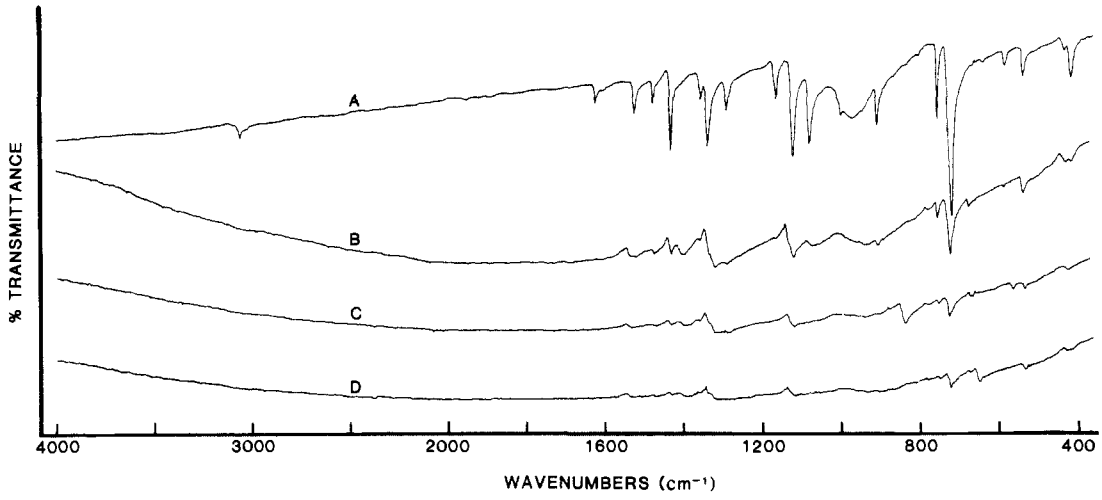

Figure 1. Transmission infrared spectra as KBr pellets of: (A) $[Si(Pc)O]_n$, (B) $\{[Si(Pc)O](BF_4)_{0.36}\}_n$, (C) $\{[Si(Pc)O](PF_6)_{0.36}\}_n$, (D) $\{[Si(Pc)O](SbF_6)_{0.36}\}_n$.

the entire spectrometer cavity, thus eliminating any dependence of instrument response on sample position. We found this technique for measuring absolute susceptibility to be considerably less accurate than the SQUID susceptometer (vide infra). Especially at low temperatures where DPPH is reported to exhibit pronounced Curie-Like behavior,[12b] attempts to ratio exact intensities must necessarily incur significant error.

Static Magnetic Susceptibility Measurements. Static magnetic susceptibilities were measured from 6–340 K by using a S.H.E. VTS-10 SQUID susceptometer. Procedures and precautions were as described previously.[7c] The use of unsublimed $Si(Pc)Cl_2$ in the $[Si(Pc)O]_n$ synthesis was found to introduce ferromagnetic impurities. The diamagnetic correction for $[Si(Pc)O]_n$, -4.455×10^{-4} emu mol^{-1}, was made as described previously.[7c] The core diamagnetic corrections for the counterions were estimated from tabulated Pascal constants: -0.442×10^{-4} emu mol^{-1} (BF_4^-), -0.67×10^{-4} emu mol^{-1} (PF_6^-), and -0.80×10^{-4} emu mol^{-1} (SbF_6^-).[13] The Curie-like components of all variable temperature data sets were analyzed in a χ vs. $1/T$ format by using linear regression techniques.

Reflectance Spectroscopy. Specular reflectance measurements in the 50–50 000 cm^{-1} range were made with the Perkin-Elmer and Zeiss instrumentation described previously.[7c] Samples were prepared by pressing the samples under 8–10 tons of pressure into disks of 13.0-mm diameter and 0.5–2.0-mm thickness. The variation in reflectance characteristics observed between different samples pressed from the same $\{[Si(Pc)O]X_y\}_n$ batch was insignificant. Samples used for detailed quantitative analysis were checked for preferential crystallite orientation by using X-ray diffraction techniques.[14] Thus, the pellets were cut into several pieces and diffraction patterns were recorded for the faces (perpendicular to the compression direction) and the edges (parallel to the compression direction). The orientation information can be expressed as the mean-square cosine of the angle (α) between the crystallographic c axis (the macrocycle stacking direction) and the compression direction (z), $\langle\cos^2 \alpha_{c,z}\rangle$.[14b,c] This parameter can be calculated by comparing the relative intensities of certain characteristic reflections (e.g., 002) and considering the various possible orientation spheres.

Charge Transport Measurements. Direct current electrical conductivity measurements were obtained from 4.2 to 320 K with use of the computer-controlled data acquisition and analysis system described elsewhere.[7c,8c,15] Samples were examined as pressed pellets with contact techniques and measurement precautions noted earlier.[7c,8c] Typically, 3–4 separate variable temperature runs were carried out for each specimen to check for reproducibility and reversibility. At a given temperature, reproducibility was within 5%.

Thermal Analysis. Thermogravimetric analysis (TGA) studies were performed under nitrogen on a Perkin-Elmer TGS-2 instrument with interfaced data system. Heating rates were 10 or 20 °C min^{-1}.

Results

In comparing the properties of the present $\{[Si(Pc)O]X_y\}_n$ materials, $X^- = BF_4^-$, PF_6^-, SbF_6^-, to those of the best-characterized halogenated analogues, $\{[Si(Pc)O](I_3)_y\}_n$,[7c] several issues are of crucial importance. First, whether macrocycle oxidation is actually occurring in the present systems and the ultimate degree of partial oxidation achievable (ρ) are essential descriptors of the doping chemistry (eq 1). Also of interest are the structures of the doped polymers and whether the doping process is homogeneous, i.e., whether dopant species are distributed uniformly throughout the solid as doping progresses or whether discrete phases of discrete structure and stoichiometry coexist. Given this information, it is next important to examine, via the magnetic, optical, and transport properties, the electronic and electrical properties of the partially oxidized $[Si(Pc^{\rho+})O]_n$ array and how they vary with counterion. Finally, these results will be compared to those for the iodinated system, and the phenomenology discussed in terms of what is presently known about stacked molecular systems[2] and other electrically conductive doped polymers.[2a,d,16]

Doping Chemistry. The synthetic route shown in eq 1, utilizing as polymerized (orthorhombic) $[Si(Pc)O]_n$ and NO^+ as the oxidizing agent, was employed to introduce BF_4^-, PF_6^-, and SbF_6^- counterions. An alternative electrochemical procedure is also applicable.[17] By varying the NOX;Si(Pc)O stoichiometry and reaction time, a wide range of y can be introduced in the resulting $\{[Si(Pc)O]X_y\}_n$ materials. However, regardless of the reaction time and the molar excess (up to two–threefold) of nitrosonium salt employed, the maximum y achieved for all three X counterions is invariably found to be 0.36 ± 0.03 by elemental analysis. This result indicates that $\rho = 0.36 \pm 0.03$, in remarkably close similarity to the value of $\rho = 0.37 \pm 0.03$ found for oxidation with iodine ($\{[Si(Pc)O^{+0.37}](I_3^-)_{0.37}\}_n$) and bromine ($\{[Si(Pc)O^{+0.37}](Br_3^-)_{0.37}\}_n$.[7c]

As judged by appearance and various physical properties (e.g., conductivity) as a function of time, the $\{[Si(Pc)O]X_y\}_n$ materials appear to be stable in air at room temperature for extended periods. The halogenated polymers were found to exhibit similar behavior. Survey thermogravimetric analysis measurements (N_2, 10–20 °C min^{-1}) on $\{[Si(Pc)O](PF_6)_{0.36}\}_n$ and $\{[Si(Pc)O]$-

(13) (a) Earnshaw, A. *Introduction to Magnetochemistry*; Academic Press: London, 1968; pp 4–8. (b) Mulay, L. N. In *Theory and Applications of Molecular Diamagnetism*; Mulay, L. N., Boudreaux, E. A., Eds.; Wiley-Interscience: New York, 1976; Chapter 5.3.

(14) (a) Klug, H. P.; Alexander, L. E. *X-ray Diffraction Procedures for Polycrystalline and Amorphous Materials*; Wiley-Interscience: New York, 1974; Chapter 8. (b) Alexander, L. E. *X-ray Diffraction Methods in Polymer Science*; Wiley: New York, 1969; pp 209–240. (c) Alexander, L. E. *X-ray Diffraction Methods in Polymer Science*; Wiley: New York, 1969; pp 241–252.

(15) Lyding, J. W.; Marcy, H. O.; Marks, T. J.; Kannewurf, C. R., submitted for publication.

(16) (a) Wynne, K. J.; Street, G. B. *Ind. Eng. Chem. Prod. Res. Devel.* **1982**, *21*, 23–28. (b) Baughman, R. H.; Bredas, J. L.; Chance, R. R.; Elsenbaumer, R. L.; Shacklette, L. W. *Chem. Rev.* **1982**, *82*, 209–222. (c) Wegner, G. *Angew. Chem., Int. Ed. Eng.* **1981**, *20*, 361–381. (d) Duke, C. G.; Gibson, H. W. In *Kirk-Othmer Encyclopedia of Chemical Technology*, 3rd ed.; John Wiley: New York, 1982; Vol. 18, pp 755–793. (e) *Conductive Polymers*; Seymour, R. B., Ed.; Polymer Science and Technology Series; Plenum Press: New York, 1981; Vol. 16.

(17) (a) Gaudiello, J. G.; Marcy, H. O.; McCarthy, W. J.; Moguel, M. K.; Kannewurf, C. R.; Marks, T. J. *Synth. Metals* **1986**, *15*, 115–128. (b) Gaudiello, J. G.; Almeida, M.; Marks, T. J.; McCarthy, W. J.; Butler, J. C.; Kannewurf, C. R. *J. Phys. Chem.*, in press.

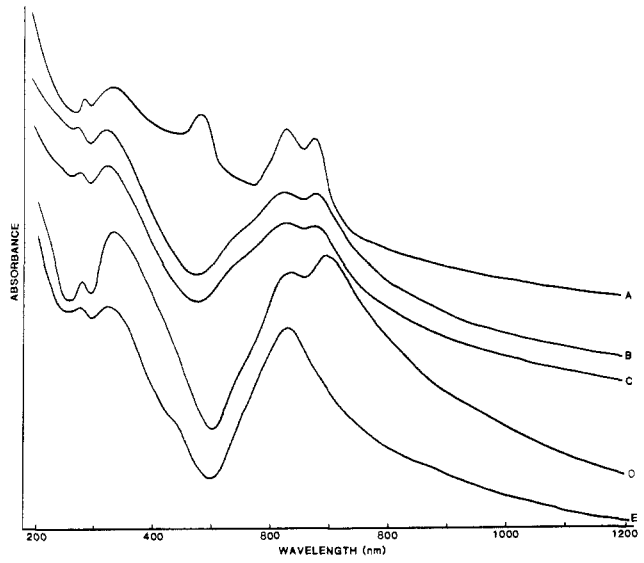

Figure 2. Transmission optical spectra as Nujol mulls of (A) $\{[Si(Pc)O](I_3)_{0.37}\}_n$, (B) $\{[Si(Pc)O](SbF_6)_{0.36}\}_n$, (C) $\{[Si(Pc)O](PF_6)_{0.36}\}_n$, (D) $\{[Si(Pc)O](BF_4)_{0.36}\}_n$, (E) $[Si(Pc)O]_n$.

Table I. Powder EPR Data for Doped $[Si(Pc)O]_n$ Polymers

compound	temp (K)	g	Γ^a (G)
$\{[Si(Pc)O](BF_4)_{0.36}\}_n$	298	2.0022	0.363
$\{[Si(Pc)O](PF_6)_{0.36}\}_n$	298	2.0036	0.835
$\{[Si(Pc)O](SbF_6)_{0.36}\}_n$	298	2.0024	2.25
$\{[Si(Pc)O](I_3)_{0.37}\}_n$[b]	298	2.0054	2.90
	77	2.0047	3.10

[a] Observed line width. [b] From ref 7c.

$(SbF_6)_{0.36}\}_n$ showed weight loss of only ca. 10% up to 360 °C. In contrast, halogen loss from $\{[Si(Pc)O](I_3)_{0.37}\}_n$ is considerably greater at these temperatures.[18]

That π electron oxidation of the Si(Pc) macrocycle is involved in this doping chemistry is evident from several lines of evidence. Transmission infrared spectra (e.g., Figure 1) reveal the characteristic conduction electron absorption of molecular "metals" and most electrically conductive polymers as well as the halogenated $[Si(Pc)O]_n$ materials,[7c,8a,19] Other than a diminution in intensity upon progressive doping, there are no discernible displacements in Si–O backbone or characteristic Pc skeletal modes. Furthermore, no new infrared-active modes are visible which could be identified with a decomposition product.

As discussed previously, the optical spectra of $[Si(Pc)O]_n$ oligomers and polymers can be understood in terms of a "four orbital" π electronic structure,[7c,20,21] modified by the proximate π systems of cofacial M(Pc) neighbors.[22] In case of the $[Si(Pc)O]_n + I_2$ reaction, it was noted that incremental iodination resulted in additional long wavelength (ca. 680 nm) absorption in the region of the Pc $\pi \rightarrow \pi^*$ "Q band" (HOMO → LUMO). Such a splitting and red shifting of the Q band is known to

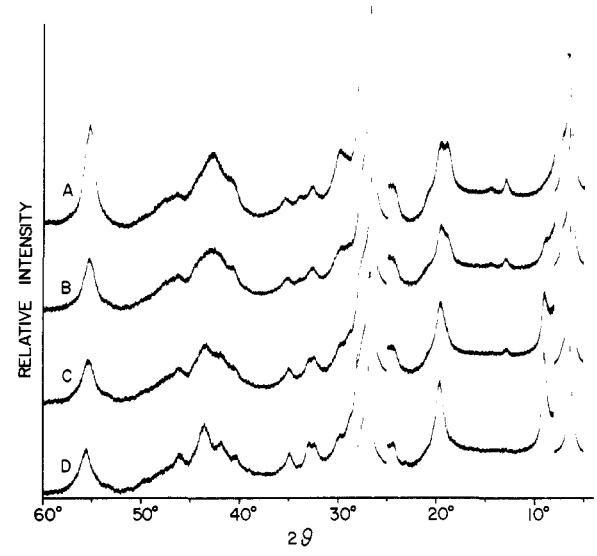

Figure 3. X-ray powder diffractometric study of the progressive doping of $[Si(Pc)O]_n$ with $NO^+BF_4^-$: (A) $y = 0.0$, vertical scale 5–8°, 20 kcps; 8–25°, 2 kcps; 25–28°, 10 kcps; 28–60°, 2 kcps. (B) $y = 0.12$, vertical scale 5–8°, 20 kcps; 8–25°, 2 kcps; 25–28°, 10 kcps; 28–60°, 2 kcps. (C) $y = 0.20$, vertical scale 5–8°, 20 kcps; 8–25°, 2 kcps; 25–28°, 10 kcps; 28–60°, 2 kcps. (D) $y = 0.36$, vertical scale 5–8°, 10 kcps; 8–25°, 2 kcps; 25–28°, 10 kcps; 28–60°, 2 kcps.

accompany M(Pc) π cation radical formation.[7c,23] For the simplest low-dimensional phthalocyanine cation radical array, $H_2(Pc)(I_3)_{0.33}$, we have recently confirmed this assignment by polarized single crystal specular reflectance spectroscopy.[7a,24] Representative optical spectra for $\{[Si(Pc)O]X_{0.36}\}_n$ materials are shown in Figure 2. The additional Q band absorption at 680 nm is clearly evident, indicating cation-radical formation. Interestingly, the 490-nm absorption of $\{[Si(Pc)O]I_{1.1}\}_n$ is not apparent in the BF_4^-, PF_6^-, and SbF_6^- salts. This spectral feature was tentatively assigned to an $(I_3^-)_n$-centered transition[3a,7c,25] and would not be expected in the present materials (further verification of the assignment is provided by the aforementioned results on $H_2(Pc)(I_3)_{0.33}$[24]).

Electron spin resonance spectroscopy provides additional information on the nature of the $\{[Si(Pc)O]X_{0.36}\}_n$ materials. The data (Table I) reveal nearly free electron g values and largely isotropic line shapes with relatively narrow line widths; they are essentially identical with the $\{[Si(Pc)O](I_3)_{0.37}\}_n$ data.[7c] This result is consistent with the unpaired spin density residing in molecular orbitals which are largely Pc ligand in character, i.e., π cation radical in character. Furthermore, any interaction between the carriers and the off-axis counterions is rather small (but probably nonzero). Additional remarks will be made in the discussion of magnetism and band structure (vide infra).

In contrast to the above findings, attempted $NO^+BF_4^-$ doping of $[Ge(Pc)O]_n$ did not result in the development of electronic absorption in the infrared (as in the case of I_2 doping). Rather, the intensity of the antisymmetric Ge–O–Ge stretching mode at 865 cm^{-1} [7d] is greatly diminished upon incremental doping, and a number of new molecular transitions grow in. In particular, a new band at 770 cm^{-1} is possibly a Ge–F stretching mode.[26] Hence, it appears likely that destruction of the $[Ge(Pc)O]_n$

(18) Wynne, K. J.; Norr, R. S. *Mol. Cryst. Liq. Cryst.* **1982**, *81*, 243–265.
(19) (a) Bozlo, R.; Pecile, C. In ref 2e, pp 165–186. (b) Fincher, C. R., Jr.; Ozaki, M.; Heeger, A. J.; MacDiarmid, A. G. *Phys. Rev. B* **1979**, *19*, 4140–4148. (c) Wheland, R. C.; Gillson, J. L. *J. Am. Chem. Soc.* **1976**, *98*, 3916–3925. (d) Tanner, D. B.; Jacobsen, C. S.; Garito, A. F.; Heeger, A. J. *Phys. Rev. B.* **1976**, *13*, 3381–3404. (e) Perez-Albuerne, E. A.; Johnson, J., Jr.; Trevoy, D. J. *J. Chem. Phys.* **1971**, *55*, 1547–1554.
(20) (a) Marks, T. J.; Stojakovic, D. R. *J. Am. Chem. Soc.* **1978**, *100*, 1695–1705, and references therein. (b) Gouterman, M. In *The Porphyrins*; Dolphin, D., Ed.; Academic Press: New York, 1978; Vol. 3, Part A, pp 1–163.
(21) (a) Shaffer, A. M.; Gouterman, M.; Davidson, E. R. *Theor. Chim. Acta* **1973**, *30*, 9–30. (b) Schaffer, A. M.; Gouterman, M. *Ibid.* **1972**, *25*, 52–70. (c) Edwards, L.; Gouterman, M. *J. Mol. Spectrosc.* **1970**, *33*, 292–310. (d) Chen, I. *Ibid.* **1967**, *23*, 131–143.
(22) Ciliberto, E.; Doris, K. A.; Pietro, W. J.; Reisner, G. M.; Ellis, D. E.; Fragalà, I.; Herbstein, F. H.; Ratner, M. A.; Marks, T. J. *J. Am. Chem. Soc.* **1984**, *106*, 7748–7761, and references therein.
(23) (a) Cahill, A. E.; Taube, H. *J. Am. Chem. Soc.* **1951**, *73*, 2847–2851. (b) Dolphin, D.; Forman, A.; Borg, D. C.; Fajer, J.; Felton, R. H. *Proc. Natl. Acad. Sci.* **1971**, *68*, 614–618.
(24) Inabe, T.; Marks, T. J.; Burton, R. L.; Lyding, J. W.; McCarthy, W. J.; Kannewurf, C. R.; Reisner, G. M.; Herbstein, F. H. *Solid State Commun.* **1985**, *54*, 501–503.
(25) (a) Mizuno, M.; Tanaka, J.; Harada, I. *J. Phys. Chem.* **1981**, *85*, 1789–1794. (b) Gabes, W.; Stufkens, D. J. *Spectrochim. Acta* **1974**, *30A*, 1835–1851.
(26) (a) Maslowsky, E., Jr. *Vibrational Spectra of Organometallic Compounds*; John Wiley and Sons: New York, 1977; pp 65, 188, and 410. (b) Esposito, J. N.; Sutton, L. E.; Kenney, M. E. *Inorg. Chem.* **1967**, *6*, 1116–1120.

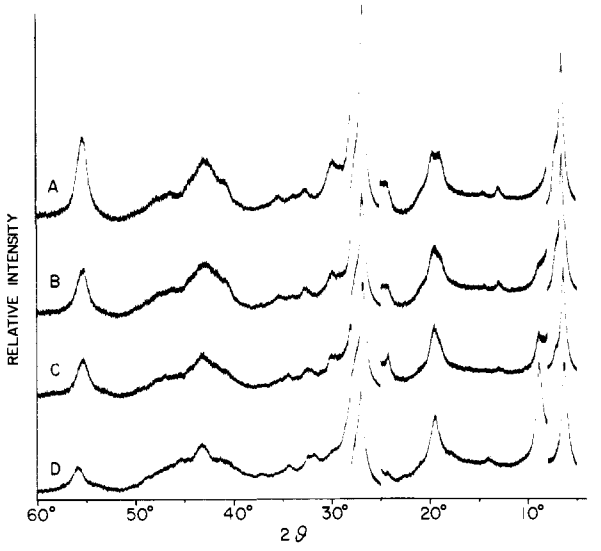

Figure 4. X-ray powder diffractometric study of the progressive doping of $[Si(Pc)O]_n$ with $NO^+PF_6^-$: (A) $y = 0.0$, vertical scale 5–8°, 20 kcps; 8–25°, 2 kcps; 25–28°, 10 kcps; 28–60°, 2 kcps. (B) $y = 0.08$, vertical scale 5–8°, 20 kcps; 8–25°, 2 kcps; 25–28°, 10 kcps; 28–60°, 2 kcps. (C) $y = 0.18$, vertical scale 5–8°, 20 kcps; 8–25°, 2 kcps; 25–28°, 10 kcps; 28–60°, 2 kcps. (D) $y = 0.36$, vertical scale 5–8°, 10 kcps; 8–25°, 2 kcps; 25–28°, 10 kcps; 28–60°, 2 kcps.

backbone occurs upon oxidation with $NO^+BF_4^-$.

X-ray Diffraction. Doping Homogeneity and Crystal Structure. For the $[Si(Pc)O]_n + I_2$ system, the observation of a growing in of $\{[Si(Pc)O](I_3)_{0.37}\}_n$ product reflections and a simultaneous diminution of $[Si(Pc)O]_n$ starting material reflections upon incremental halogenation (rather than a continuous/monotonic displacement of the lattice parameters[27a]) argued strongly for the inhomogeneity of the doping process (at least on the coherence length of the X-ray diffraction experiment).[7c,27b] At intermediate doping levels, the diffraction pattern can be reproduced by suitable mechanical admixture of the fully doped and undoped phases. Moreover, many other physical properties of the $\{[Si(Pc)O](I_3)_y\}_n$ system can be understood largely in terms of inhomogeneous mixtures of $[Si(Pc)O]_n$ and $\{[Si(Pc)O]I_{1.1}\}_n$.[7c] As can be seen in Figures 3 and 4, significant changes in the orthorhombic[7d] $[Si(Pc)O]_n$ crystal structure accompany incremental NOX doping. Although not as elaborate as for iodination, several distinctive features in the diffraction patterns strongly suggest an inhomogeneous process. Most evident is the development of the reflection at $2\theta = 9°$ which is only present in the doped $X^- = BF_4^-$, PF_6^-, and SbF_6^- materials and will be seen to be sensitive to the electron density in the counterion "tunnels" (vide infra). In addition, doping is accompanied by the simultaneous diminution of the orthorhombic $[Si(Pc)O]_n$ reflections at $2\theta \approx 12$, 18, and 34°. Throughout the doping process, the 9, 12, 18, and 34° reflections do not undergo a detectable displacement in 2θ position, and at intermediate doping levels, the observed diffraction patterns are simple superpositions of the fully doped and undoped patterns. Diffraction patterns of the fully doped $\{[Si(Pc)O]X_{0.36}\}_n$ materials are compared for $X^- = BF_4^-$, PF_6^-, and SbF_6^- in Figure 5. As was noted for the halogen-doped materials,[7c,d] the X-ray line widths are consistent with the observed[7c] $[Si(Pc)O]_n$ degree of polymerization.

Other workers have reported that similar $\{[Si(Pc)O]X_y\}_n$ materials prepared by galvanostatic doping of pressed pellets exhibit Debye–Scherrer diffraction patterns virtually identical with those of undoped $[Si(Pc)O]_n$.[28] The implication is that introduction

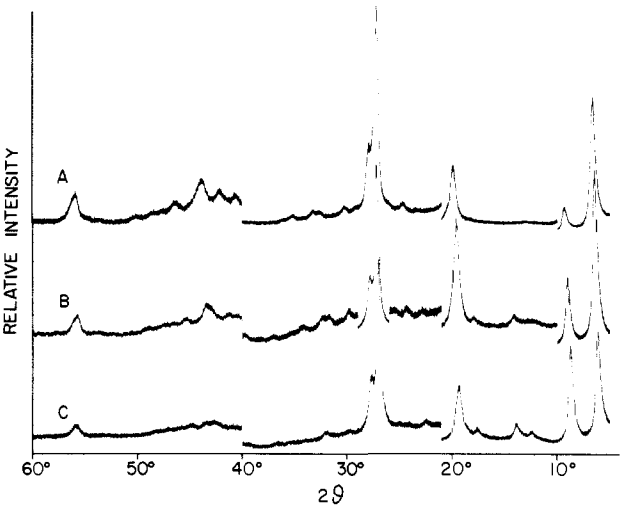

Figure 5. Comparative X-ray powder diffractometric traces of the following: (A) $\{[Si(Pc)O](BF_4)_{0.36}\}_n$, vertical scale 5–10°, 10 kcps; 10–21°, 4 kcps; 21–40°, 8 kcps; 40–60°, 4 kcps. (B) $\{[Si(Pc)O](PF_6)_{0.36}\}_n$, vertical scale 5–10°, 8 kcps; 10–26°, 4 kcps; 26–29°, 8 kcps; 29–60°, 4 kcps. (C) $\{[Si(Pc)O](SbF_6)_{0.36}\}_n$, vertical scale: 5–40°, 4 kcps; 40–60, 2 kcps.

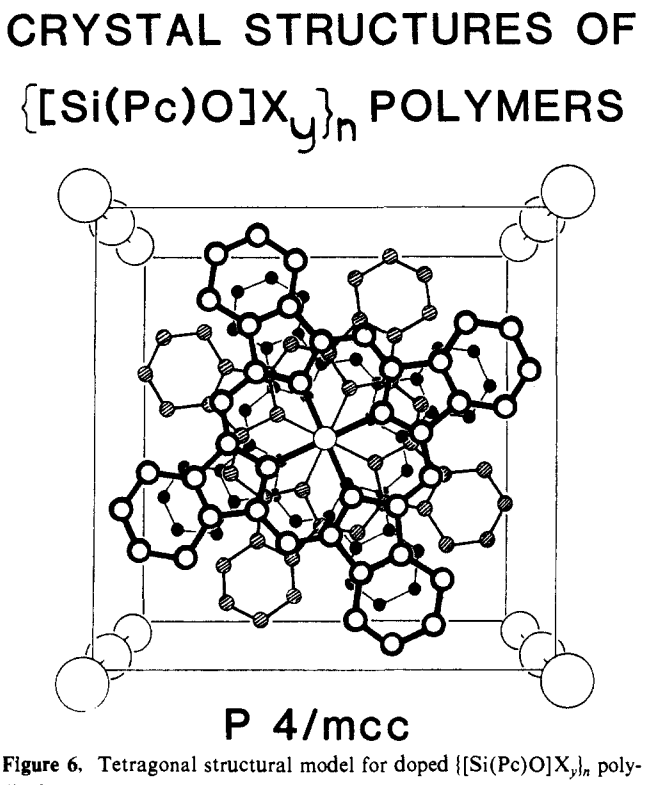

Figure 6. Tetragonal structural model for doped $\{[Si(Pc)O]X_y\}_n$ polymers.

of the dopant counterions does not appreciably change the packing of the polymer stacks, hence the crystal structure. Close examination of Figures 3, 4, and 5 (results for our electrochemically doped $y = 0.36$ materials are very similar[17]) indicates that the diffraction patterns of undoped and doped phases are similar but only in a superficial sense. We suspect that the resolution and dynamic range limitations of the photographic technique obscured the differences in diffraction patterns, especially at low 2θ values. The crystal structures of the undoped (orthorhombic) and doped (tetragonal) phases will be seen to differ considerably.

The analysis of the $\{[Si(Pc)O]X_{0.36}\}_n$ crystal structures utilized the same numerical techniques as employed for the corresponding $[M(Pc)O]_n$, $\{[M(Pc)O](Br_3)_{0.37}\}_n$, and $\{[M(Pc)O](I_3)_{0.37}\}_n$ materials.[7c] In those cases, computer simulation procedures were employed to generate theoretical diffraction patterns for trial structures derived from a broad data base of structurally well-characterized model compounds. Excellent agreement was ob-

(27) (a) An example of a homogeneous transformation in a conductive polymer is the cis to trans isomerization of polyacetylene: Robin, P.; Pouget, J. P.; Cômes, R.; Gibson, H. W.; Epstein, A. J. *Phys. Rev. B* **1983**, *27*, 3938–3941. (b) Further verification of the inhomogeneity is provided by TEM results: Zhou, X.; Carr, S. H.; Marks, T. J., submitted for publication.

(28) Orthmann, E. A.; Enkelmann, V.; Wegner, G. *Makromol. Chem. Rapid Commun.* **1983**, *4*, 687–692.

Table II. Crystallographic Data for Partially Oxidized Phthalocyanine Materials

compound	space group	Z	cell parameters (Å)	density (g cm^{-3}) calcd	density (g cm^{-3}) found	interplanar spacing (Å)	staggering angle (deg)
$\{[Si(Pc)O](BF_4)_{0.36}\}_n$[a]	$P4/mcc$	2	a = 13.70 (7) c = 6.58 (4)	1.581 (21)	1.545 (6)	3.29 (2)	40 (2)
$\{[Si(Pc)O](PF_6)_{0.36}\}_n$[a]	$P4/mcc$	2	a = 13.98 (6) c = 6.58 (4)	1.573 (19)	1.563 (7)	3.29 (2)	40 (2)
$\{[Si(Pc)O](SbF_6)_{0.36}\}_n$[a]	$P4/mcc$	2	a = 14.31 (4) c = 6.58 (4)	1.582 (14)	1.591 (5)	3.29 (2)	40 (2)
$Ni(Pc)(BF_4)_{0.35}$[b]	$P4/mcc$	2	a = 13.97 (2) c = 6.48 (1)			3.240 (5)	40 (1)
$Ni(Pc)(ClO_4)_{0.40}$[c]	$P4/mcc$	2	a = 13.957 (3) c = 6.4672 (9)			3.234 (5)	39.3
$\{[Si(Pc)O](I_3)_{0.37}\}_n$[d]	$P4/mcc$	2	a = 13.97 (5) c = 6.60 (4)	1.802 (24)	1.744 (10)	3.30 (2)	39 (3)
$\{[Si(Pc)O](Br_3)_{0.37}\}_n$[d]	$P4/mcc$	2	a = 13.97 (5) c = 6.60 (4)			3.30 (2)	39 (3)
$\{[Ge(Pc)O](I_3)_{0.36}\}_n$[d]	$P4/mcc$	2	a = 13.96 (5) c = 6.96 (4)	1.805 (23)	1.774 (10)	3.48 (2)	40 (4)
$H_2(Pc)(I_3)_{0.33}$[e]	$P4/mcc$	2	a = 13.979 (6) c = 6.502 (3)			3.251 (2)	40 (1)
$Ni(Pc)(I_3)_{0.33}$[f]	$P4/mcc$	2	a = 13.936 (6) c = 6.488 (3)	1.84	1.78 (4)	3.244 (2)	39.5
$[Si(Pc)O]_n$[g]	$Ibam$	4	a = 13.80 (5) b = 27.59 (5) c = 6.66 (4)	1.458 (21)	1.432 (10)	3.33 (2)	39 (3)

[a] This work. [b] Reference 30. [c] Reference 29a. [d] Reference 7c. [e] Reference 22. [f] Reference 29. [g] Reference 7d.

tained between the powder-derived structural conclusions and single-crystal results on related species, e.g., $[Si(Pc)O]_n$[7d] and ROSi(Pc)OSi(Pc)OR (R = Si[C(CH$_3$)$_3$](CH$_3$)$_2$)[22]; $\{[M(Pc)O](I_3)_{0.37}\}_n$,[7c] $Ni(Pc)(ClO_4)_{0.40}$,[29a] $Ni(Pc)(BF_4)_{0.35}$,[10c] $Ni(Pc)(I_3)_{0.33}$,[29b] and $H_2(Pc)(I_3)_{0.33}$[24].

The structural model for the $\{[Si(Pc)O]X_{0.36}\}_n$ materials was the tetragonal configuration shown in Figure 6. This is essentially the $\{[Si(Pc)O](I_3)_{0.37}\}_n$ motif which has also been found in recent single-crystal diffraction investigations of $Ni(Pc)(BF_4)_{0.35}$[10c,30] and $Ni(Pc)(ClO_4)_{0.40}$.[29a] Theoretical calculations were carried out by sequentially varying interplanar spacing, ring–ring staggering angle (ϕ in D), the angle between the Pc trans N–M–N vector and the

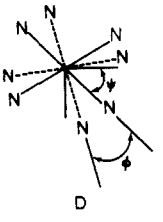

D

unit cell edge (ψ in D), and various anion positions/orientations. For $X^- = BF_4^-$ and PF_6^-, the calculated patterns were found not to be particularly sensitive to the anion positions or orientations (due to the small scattering factors) but quite sensitive to ϕ. The best fit was found for $\phi = 40° \pm 2°$ in both compounds. In the case of $X^- = SbF_6^-$, the sensitivity of the diffraction pattern to the anion positions is much higher than for the lighter counterions. In particular, the intensity ratio of the 002 and 102 reflections was found to be highly dependent upon the anion positions. As can be seen in Figure 7, partially ordered arrangements of the octahedral anion (0.36 occupation) with locations at either Z = $^1/_4$ and $^3/_4$ (Figure 7A) or at Z = 0 and $^1/_2$ (Figure 7B) result in too strong or too weak 102 reflections, respectively. The best fit was found for the disordered model shown in Figure 7C. It was also found that the orientation of the SbF_6^- anion has only minor effects on the calculated diffraction patterns. Of course, since the anion tunnel has a crystallographically imposed fourfold axis, the tetrahedral BF_4^- ion would necessarily be disordered.

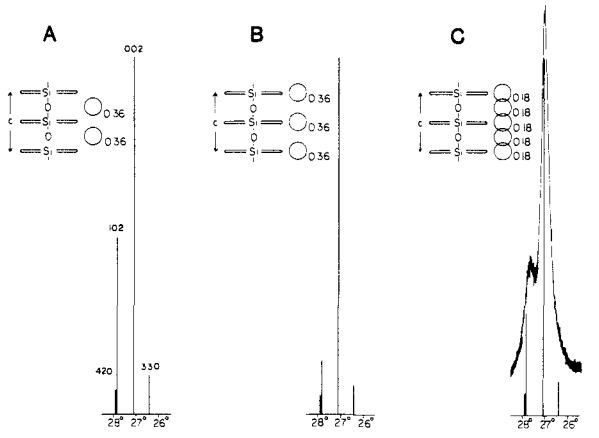

Figure 7. Calculated and experimental X-ray diffraction patterns for $\{[Si(Pc)O](SbF_6)_{0.36}\}_n$ showing the effects of different assumed SbF_6^- positions along the crystallographic c direction: (A) 0.36 occupation of SbF_6^- at Z = $^1/_4$ and $^3/_4$; (B) 0.36 occupation of SbF_6^- at Z = 0 and $^1/_2$; (C) 0.18 occupation of SbF_6^- at Z = 0, $^1/_4$, $^1/_2$, and $^3/_4$.

In all cases, the data are in best agreement with positionally and orientationally disordered BF_4^-, PF_6^-, and SbF_6^- counterions.

A comparison of experimental and calculated diffraction patterns for the three $\{[Si(Pc)O]X_{0.36}\}_n$ materials is shown in Figure 8. The agreement is very good.[31] Derived cell parameters and experimental density data (which are in good agreement with calculated densities) are set out in Table II and are compared there to results for both $[Si(Pc)O]_n$ and the halogenated analogues. It can be seen for all $[Si(Pc^{o+})O]_n$ materials that, within experimental error, the Pc–Pc eclipsing angles are identical as is the characteristic contraction in the Si(Pc)–Si(Pc) interplanar spacing upon oxidation. The a parameters, which reflect the lateral interchain separations, are a readily understood[6b] function of the anion sizes. However, an interesting structural departure from the halogenated polymers is evident when the disparate spatial requirements of I_3^- (1.1 per $\{Si(Pc)O\}_3$ fragment) vs. BF_4^-, PF_6^-, and SbF_6^- (1.1 per $\{Si(Pc)O\}_3$ fragment) are considered. A very rough estimate of the spatial requirements of the latter three ions can be obtained by assuming spherical symmetry and adding twice the F van der

(29) (a) Kanatzidis, M.; Almeida, M.; McCarthy, W. J.; Kannewurf, C. R.; Marks, T. J., submitted for publication. (b) Schramm, C. S.; Scaringe, R. P.; Stojakovic, D. R.; Hoffman, B. M.; Ibers, J. A.; Marks, T. J. *J. Am. Chem. Soc.* **1980**, *102*, 6702–6713.

(30) (a) Inabe, T.; Nakamura, S.; Liang, W.-B.; Marks, T. J.; McCarthy, W. J.; Kannewurf, C. R.; Imaeda, K.-I., submitted for publication. (b) Inabe, T.; Reisner, G. M.; Herbstein, F. H.; Marks, T. J., manuscript in preparation.

(31) Since the calculations do not include Debye–Waller (temperature) factors, theoretical reflection intensities at larger values of 2θ are stronger than the observed intensities.

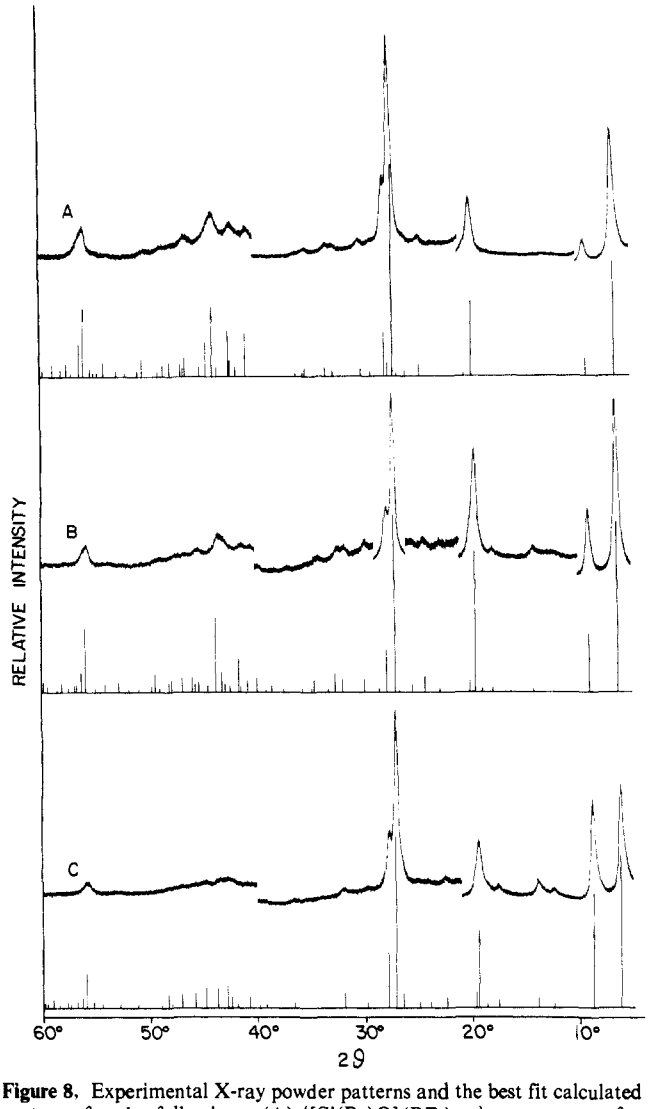

Figure 8. Experimental X-ray powder patterns and the best fit calculated patterns for the following: (A) $\{[Si(Pc)O](BF_4)_{0.36}\}_n$, parameters for simulation $P4/mcc$, a = 13.81, c = 6.58 Å, staggering angle 40°; (B) $\{[Si(Pc)O](PF_6)_{0.36}\}_n$, parameters for simulation $P4/mcc$, a = 13.98, c = 6.58 Å, staggering angle 40°; (C) $\{[Si(Pc)O](SbF_6)_{0.36}\}_n$ parameters for simulation $P4/mcc$, a = 14.31, c = 6.58 Å, staggering angle 40°. Vertical scale of experimental patterns is the same as in Figure 5. Vertical scale of simulation is normalized to experimental conditions.

Waals radius[32] to twice the sum of the appropriate ionic radii,[33] The resulting "van der Waals diameters" are calculated to be ca. 5.9 (BF_4^-), 6.4 (PF_6^-), and 6.9 Å (SbF_6^-). In comparison, the I(1)–I(3) distance in typical I_3^- ions is on the other order of ca. 5.8 Å,[3a] and the "van der Waals length" of I_3^- (5.8 Å + twice the iodine van der Waals radius[32]) would be on the order of 9.8–10 Å. Thus, there is clearly considerably empty space in the counterion "tunnels" of the BF_4^-, PF_6^-, and SbF_6^- salts. It is therefore also evident that the degree of partial oxidation achieved has not been limited in these materials solely by the population of anions which could be accommodated in the counterion "tunnels".

Since the synthesis solvent, CH_2Cl_2, is comparable in size to these ions, the question arises as to whether it might be trapped in the lattice (calculations indicate that up to ca. 0.5 CH_2Cl_2/Si(Pc) could be accommodated in the X^- = BF_4^- material). However, neither elemental analyses, density measurements, nor the X-ray data (the $2\theta \approx 9°$ reflection is quite sensitive to the electron density in the counterion "tunnels"—cf., Figure 8) give

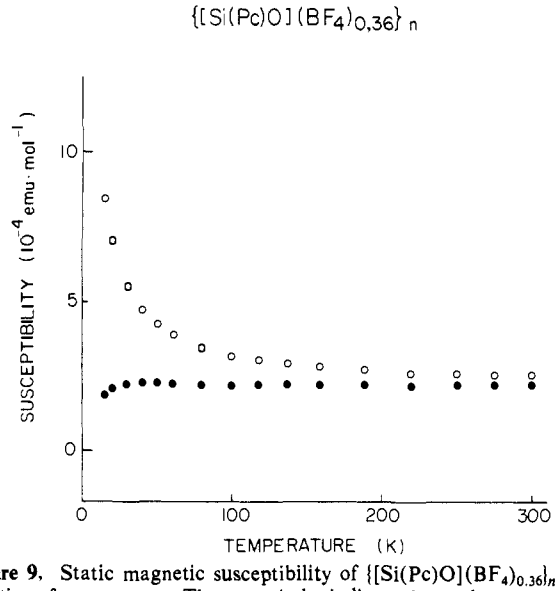

Figure 9. Static magnetic susceptibility of $\{[Si(Pc)O](BF_4)_{0.36}\}_n$ as a function of temperature. The open circles indicate the total paramagnetic susceptibility including the Curie component, and the closed circles indicate the Pauli-like component.

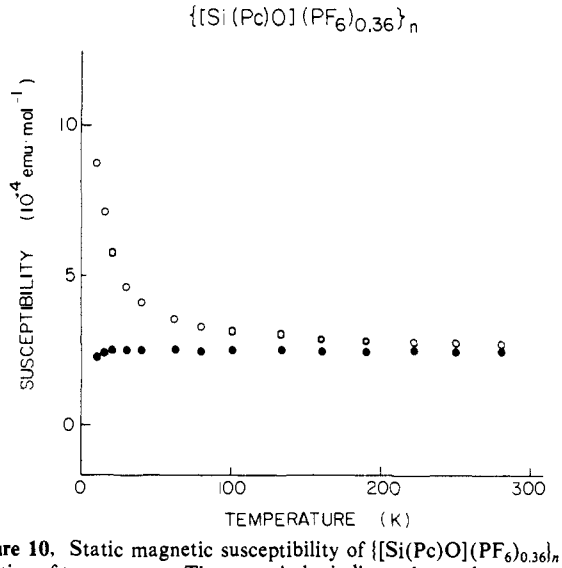

Figure 10. Static magnetic susceptibility of $\{[Si(Pc)O](PF_6)_{0.36}\}_n$ as a function of temperature. The open circles indicate the total paramagnetic susceptibility including the Curie component, and the closed circles indicate the Pauli-like component.

any indication of included CH_2Cl_2 molecules.

Magnetic Properties of $\{[Si(Pc)O]X_y\}_n$ Polymers. The static magnetic susceptibilities of the doped polymers $\{[Si(Pc)O](BF_4)_{0.36}\}_n$, $\{[Si(Pc)O](PF_6)_{0.36}\}_n$, and $\{[Si(Pc)O](SbF_6)_{0.36}\}_n$ were studied as a function of temperature by using a highly sensitive SQUID susceptometer. Procedures for making diamagnetic corrections[7c] are outlined in the Experimental Section. Typical susceptibility data are shown in Figures 9 and 10. As found for the halogen-doped $[M(Pc)O]_n$ materials as well as in our work on $H_2(Pc)(I_3)_{0.33}$ and $Ni(Pc)(I_3)_{0.33}$,[7c,23] the data exhibit "Curie tailing" at low temperatures. This is a common feature (i.e., $\chi \sim T^{-\alpha}$, $\alpha \approx 0.8$–1.0) in the susceptibilities of many molecular and polymeric conductors and is usually ascribed to impurities, defects, or disorder.[34,35] If the origin is assumed to be localized $S = {}^1/_2$,

(32) Huheey, J. E. *Inorganic Chemistry*, 3rd ed.; Harper and Row: New York, 1983; pp 258–259.
(33) Shannon, R. D. *Acta Crystallogr., Sect. A: Cryst. Phys., Diffr., Theor. Gen. Crystallogr.* **1976**, *A32*, 751–767.

(34) (a) Scott, J. C.; Garito, A. F.; Heeger, A. J. *Phys. Rev. B* **1974**, *10*, 3131–3139. (b) Isett, L. C. *Phys. Rev. B* **1978**, *18*, 439–447. (c) Delhaes, P.; Coulon, C.; Flandrois, S.; Hilti, B.; Mayer, C. W.; Rihs, G.; Rivory, J. *J. Chem. Phys.* **1980**, *73*, 1452–1463. (d) Martinsen, J.; Palmer, S. M.; Tanaka, J.; Greene, R. C.; Hoffman, B. M. *Phys. Rev. B* **1984**, *30*, 6269–6276. (e) Takahashi, M.; Sugano, T.; Kinoshita, M. *Bull. Chem. Soc. Jpn.* **1984**, *57*, 26–35, and references therein.

Table III. Magnetic Data for Partially Oxidized Phthalocyanine Materials

compound	χ^{Pauli} (emu mol^{-1})	spins/ M(Pc)	4t (eV)	interplanar spacing (Å)	enhancement[a]
$\{[Si(Pc)O](BF_4)_{0.36}\}_n$[b]	2.22 (6) × 10^{-4}	0.18 (1)	0.35 (1)	3.29 (2)	1.8
$\{[Si(Pc)O](PF_6)_{0.36}\}_n$[b]	2.49 (7) × 10^{-4}	0.19 (1)	0.31 (1)	3.29 (2)	2.0
$\{[Si(Pc)O](SbF_6)_{0.36}\}_n$[b]	2.22 (7) × 10^{-4}	0.18 (1)	0.35 (1)	3.29 (2)	1.8
$\{[Si(Pc)O](I_3)_{0.37}\}_n$[c]	2.35 (11) × 10^{-4}	0.18 (1)	0.32 (3)	3.30 (2)	1.9
$\{[Ge(Pc)O](I_3)_{0.37}\}_n$[c]	2.70 (10) × 10^{-4}	0.21 (1)	0.28 (2)	3.48 (2)	1.7
$Ni(Pc)(I_3)_{0.33}$[c]	1.90 (8) × 10^{-4}	0.15 (1)	0.43 (3)	3.244 (2)	2.3
$H_2(Pc)(I_3)_{0.33}$[d]	2.21 (5) × 10^{-4}	0.18 (1)	0.38 (1)	3.251 (3)	3.1
$Ni(Pc)(BF_4)_{0.33}$[e]	1.30 (4) × 10^{-4}	0.11 (1)	0.64 (3)	3.24 (1)	2.0

[a] $t_{optical}/t_{magnetic}$. [b] This work. [c] Reference 7c. [d] Reference 24. [e] Reference 10c.

g = 2.00 impurities, the percentage of Curie-like species can be obtained from the susceptibility data via linear regression analysis.[7c,35c] For doped $[Si(Pc^{\rho+})O]_n$ materials, this impurity percentage has been found to vary from batch to batch of the material and not to be correlated with the doping level.[7c] For the samples of Figures 9 and 10, the percentage of Curie-like impurity is found (assuming α = 1.0) to be 2.6% and 1.7%, respectively. These quantities are in the range found for $\{[Si(Pc)O](I_3)_{0.37}\}_n$ and related materials, arguing that surface iodine loss is not the principal cause of the Curie-like centers.

Subtraction of the Curie-like components, which dominate at lower temperatures, from the paramagnetic susceptibilities yields susceptibilities which are only weakly dependent upon temperature (filled circles in Figures 9 and 10), i.e., are decidedly Pauli-like.[34,36] Similar magnetic behavior has been observed for $\{[M(Pc)O](I_3)_y\}_n$, M = Si, Ge[7c], $H_2(Pc)(I_3)_{0.33}$,[24] $Ni(Pc)(I_3)_{0.33}$,[7c,34d] and $Ni(Pc)(BF_4)_{0.35}$,[10c,30] although such weak temperature dependence is not, in general, a characteristic of most molecular metals.[2,34] Magnetic data for the present and related partially oxidized phthalocyanine systems are compiled in Table III. Room temperature spins per M(Pc) unit have been calculated assuming isolated $S = {}^1/_2$, g = 2.00 units.[37] Most remarkable are the essentially identical Pauli-like susceptibilities for all of the $[Si(Pc^{\rho+})O]_n$ polymers—clearly the band structure is not strongly coupled to the off-axis counterions in a magnetic sense. Neither the size nor charge localization of the anion has a perceptible influence on the static susceptibility.

Verification of the above conclusions as well as additional electronic information is provided by ESR spectroscopy. Measurement of the absolute signal intensity of $\{[Si(Pc)O](BF_4)_{0.36}\}_n$ at room temperature yields a paramagnetic susceptibility that is within experimental error identical with that obtained with the SQUID susceptometer (vide supra, Table III). Furthermore, the magnitude of the ESR spin susceptibility closely parallels the SQUID data; Pauli-like behavior at higher temperaures and Curie-like behavior at lower temperatures (Figure 11A). Any separate Curie-like signal is not resolved at lower temperatures.[36b]

The ESR line widths of the $\{[Si(Pc)O]X_y\}_n$ materials are rather narrow at room temperature (Table I) and insensitive to temperature (Figure 11B). Such narrow line widths can be associated with the absence of heavy atoms in extensive communication with the carriers as is observed in organochalcogenide molecular metals (electronic relaxation via phonon-modulated spin-orbit interactions[38]) as well as with the highly unidimensional nature of the crystal and electronic structure, i.e., the interstack transfer integral (the interstack Hückel β integral), $t_\perp$, is rather small.[34e,38,39] Similar conclusions about the dimensionality were reached for $H_2(Pc)(I_3)_{0.33}$ on the basis of the anisotropy of the reflectivity and charge transport.[24] It is reasonable that the small line width differences ordered as $I_3^- > SbF_6^- > PF_6^- > BF_4^-$ reflect minor spin orbit-related interactions of the carriers with the off-axis counterions. The absence of an abrupt change in line width with temperature argues, as does the transport data (vide infra), against the occurrence of a metal-insulator transition.

Assuming a one-dimensional tight-binding band with noninteracting electrons (i.e., the Hubbard on-site Coulomb repulsion

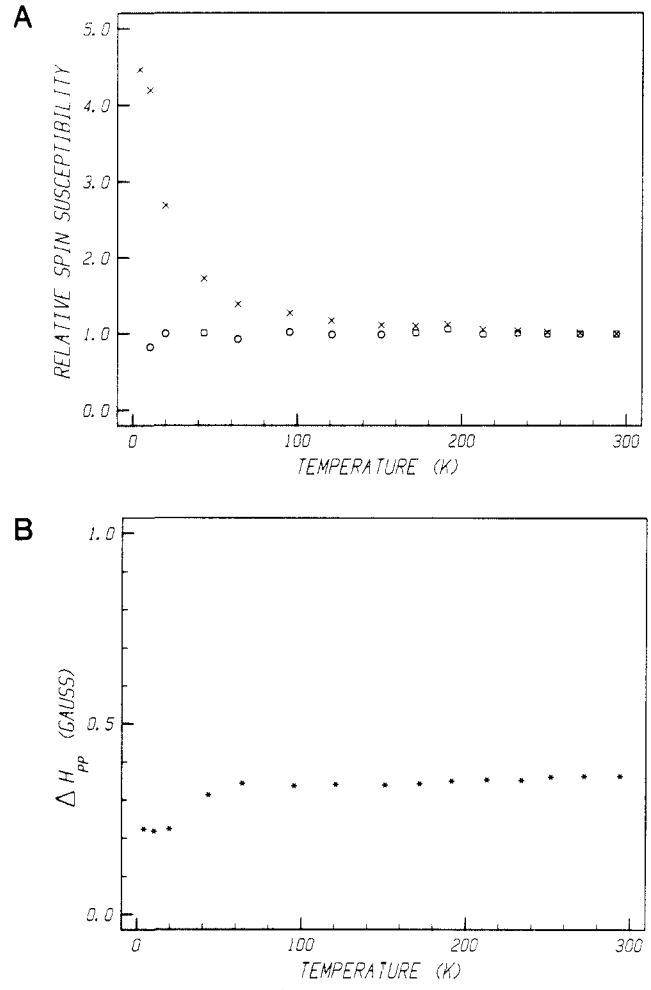

Figure 11. (A) Temperature dependence of the ESR spin susceptibility of $\{[Si(Pc)O](BF_4)_{0.36}\}_n$ ratioed to the room temperature spin susceptibility. The Pauli-like component is denoted by squares and the total spin susceptibility by X symbols. (B) Temperature dependence of the ESR signal line width for $\{[Si(Pc)O](BF_4)_{0.36}\}_n$.

(35) (a) Bailey, J. C.; Chesnut, D. B. *J. Chem. Phys.* **1969**, *51*, 5118–5128. (b) Bulaevskii, L. N.; Zvarykina, A. V.; Karimov, Yu. S.; Lyubovskii, R. C.; Shchegolev, I. F. *JETP* **1972**, *35*, 384–389. (c) Azevedo, L. J.; Clark, W. G. *Phys. Rev. B* **1977**, *16*, 3252–3258. (d) Tippie, L. C.; Clark, W. G. *Phys. Rev. B* **1981**, *23*, 5846–5853. (e) Soos, Z. G.; Bondeson, S. R. *Mol. Cryst. Liq. Cryst.* **1982**, *85*, 19–31.

(36) (a) Kittel, C. *Introduction to Solid State Physics*, 5th ed.; John Wiley: New York, 1976; Chapter 14. For other examples of Pauli-like magnetism in a molecular conductor, see ref 34c–e, and (b) Höptner, W.; Mahring, M.; von Schütz, Z. U.; Wolf, H. C.; Morra, B. S.; Enkelmann, V.; Wegner, G. *Chem. Phys.* **1982**, *73*, 253–261.

(37) Calculated from the simple Curie relationship[36a]

$$\chi = \frac{Ng^2\mu_B^2 S(S+1)}{3kT}$$

(38) Maresch, G. G.; Mehring, M.; von Schütz, J. U.; Wolf, H. C. *Chem. Phys.* **1984**, *85*, 333–340, and references therein.

(39) (a) Jérome, D. ref 2h, pp 123–142. (b) Soos, Z.; Bondeson, S. R. ref 2e, Vol. 3, pp 229–233. (c) Schultz, T. D.; Craven, R. A. ref 2i, pp 166–176, and references therein. (d) Carneiro, K.; Scott, J. C.; Engler, E. M. *Solid State Commun.* **1984**, *50*, 477–481, and references therein.

Table IV. Optical Reflectance Data for Partially Oxidized Phthalocyanine Materials[a]

compound	ω_p (eV)	τ (10^{-15} s)	ϵ_{core}	$4t$ (eV)	m^*/m_0	σ_{opt} (Ω^{-1} cm^{-1})
$\{[Si(Pc)O](BF_4)_{0.36}\}_n$[b]	0.583 (14)	5.10 (13)	2.29 (10)	0.64 (6)	2.3 (3)	400
$\{[Si(Pc)O](PF_6)_{0.36}\}_n$[b]	0.570 (19)	4.09 (13)	2.16 (12)	0.63 (6)	2.4 (3)	300
$\{[Si(Pc)O](SbF_6)_{0.36}\}_n$[b]	0.564 (19)	9.18 (33)	2.21 (13)	0.64 (6)	2.3 (3)	600
$\{[Si(Pc)O](I_3)_{0.37}\}_n$[c]	0.563 (8)	5.89 (9)	2.78 (7)	0.60 (6)	2.5 (3)	400
$\{[Ge(Pc)O](I_3)_{0.37}\}_n$[c]	0.522 (6)	3.97 (10)	2.95 (7)	0.48 (5)	2.9 (3)	200
Ni(Pc)I[c]	0.698 (7)	3.78 (4)	3.43 (7)	0.99 (9)	2.9 (2)	400

[a] Standard deviations were established by the fitting procedure. [b] This work. [c] Reference 7c.

integral, $U = 0$), it is possible to express a Pauli magnetic susceptibility in terms of the intrastack transfer integral, $t_\parallel$, as shown in eq 2.[34b,40] Here N is Avogadro's number, μ_B is the Bohr

$$\chi^P = \frac{N\mu_B{}^2}{t_\parallel \pi \sin(\pi\rho/2)} \quad (2)$$

magneton, and ρ is the degree of partial oxidation. Calculated "magnetic" bandwidths ($4t_\parallel$) are compiled in Table III. The agreement between magnetic bandwidths measured for the various $[Si(Pc^{\rho+})O]_n$ materials is very close. However, the actual magnitudes of the bandwidths are small (vide infra), and Coulomb enhancement of the susceptibility (i.e., $U = 0$ is a poor assumption)[3b,40b,41] or electron–phonon interactions[42] are possible causes.

$\{[Si(Pc)O]X_y\}_n$ Optical Reflectivity. Specular reflectance information on the X = BF_4^--, PF_6^--, and SbF_6^--containing polymers was obtained from the far-infrared to the UV on pressed polycrystalline samples. We have previously shown that when suitable corrections are made for the polycrystalline and sometimes partially anisotropic nature of such specimens, good agreement with single-crystal reflectivity data is obtained.[7c,24,43a] Spectra of the present materials along with results for $\{[Si(Pc)O](I_3)_{0.37}\}_n$ are presented in Figure 12. In all cases, the features are rather similar, with the only conspicuous differences being molecular modes assignable to BF_4^--, PF_6^--, and SbF_6^--centered excitation. Importantly, all of the spectra exhibit an edgelike feature beginning at ca. 3200 cm^{-1}.

After using X-ray diffraction data to correct for preferential crystallite orientation,[7c] the reflectance data[43b] were fit to a simple Drude (electron gas) model for the dielectric function $\epsilon(\omega)$ (eq 3).[44] Here ϵ_{core} is the dielectric constant at high frequency arising

$$\epsilon(\omega) = \epsilon_{core} - \frac{\omega_p{}^2}{\omega^2 + i\omega/\tau} \quad (3)$$

from the core polarizability, ω_p is the plasma frequency, and τ is the electronic relaxation time (for scattering near the Fermi surface). The plasma frequency can be related to the carrier density per unit volume, N_c, and the optical effective mass of the carriers, m^*, by eq 4. The majority carriers have been shown

$$\omega_p{}^2 = 4\pi N_c e^2/m^* \quad (4)$$

to be holes on the basis of thermopower data (a radical cation conductor),[17b,45] and N_c can be calculated from the experimental degree of partial oxidation, ρ, and crystallographic data. An optically derived estimate of the low frequency electrical conductivity can be obtained via eq 5. In Table IV are set out the

$$\sigma_{opt} = \omega_p{}^2\tau/4\pi \quad (5)$$

optical parameters obtained from the numerical analysis of the reflectivity data for a variety of partially oxidized phthalocyanines. Most striking is the rather close similarity of the parameters for all of the $[Si(Pc^{\rho+})O]_n$ materials, with counterion ion effects being very minor. It will also be seen in the discussion of charge transport behavior that the σ_{opt} values are realistic (vide infra).

For a simple one-dimensional tight-binding band structure, the plasma frequency can be related to the bandwidth and the interplanar Pc–Pc spacing, c, as shown in eq 6.[44] The reliability

$$4t_\parallel = \frac{\rho(\hbar\omega_p)^2}{4N_c e^2 c^2 \sin(\pi\rho/2)} \quad (6)$$

of this relationship has recently been demonstrated[22] for $[Si(Pc^{\rho+})O]_n$ systems by the good agreement in $4t$ parameters obtained from a Drude analysis of $\{[Si(Pc)O](I_3)_{0.37}\}_n$ reflectivity data, computer-analyzed gas-phase photoemission spectra of the cofacial dimer ROSi(Pc)OSi(Pc)OR (R = Si[C(CH$_3$)$_3$](CH$_3$)$_2$), and first-principles discrete variational local exchange electronic structure calculations on the cofacial dimer HOSi(Pc)OSi(Pc)OH.[22] Tight-binding bandwidth parameters for a number of

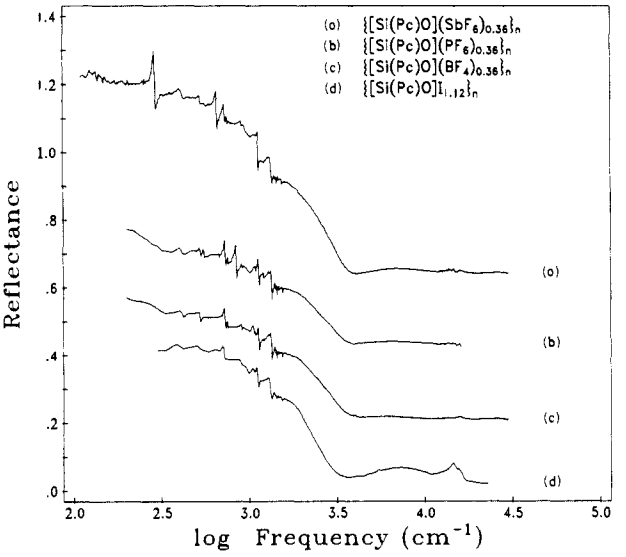

Figure 12. Optical reflectance spectra of polycrystalline samples of the conductive polymers indicated. For ease of viewing, successive spectra have been offset vertically by 20%.

(40) (a) Shiba, H. *Phys. Rev. B* **1972**, *6*, 930–938. (b) Torrance, J. B.; Tomkiewicz, Y.; Silverman, B. D. *Phys. Rev. B* **1977**, *15*, 4738–4749.

(41) (a) Mazumdar, S.; Bloch, A. N. *Phys. Rev. Lett.* **1983**, *50*, 207–211. (b) Mortensen, K.; Conwell, E. M.; Fabre, J. M. *Phys. Rev. B* **1983**, *28*, 5856–5862. (c) Coulon, C.; Delhaes, P.; Flandrois, S.; Lagnier, R.; Bonjour, E.; Fabre, J. M. *J. Phys.* **1982**, *43*, 1059–1066. (d) Mazumdar, S.; Dixit, S. N. *Phys. Rev. B* **1986**, *34*, 3683–3699.

(42) Gutfreund, H.; Entin-Wohlman, O.; Weger, M. ref 2a, Vol. 119, pp 457–466, and references therein.

(43) (a) McCarthy, W. J.; Kannewurf, C. R.; Inabe, T.; Marks, T. J.; Burton, R. L. In "Basic Properties of Optical Materials"; Feldman, A., Ed.; *NBS Spec. Publ.* (*U. S.*) 1985, No. 697, pp 54–57. (b) where $\epsilon = (\epsilon_1{}^2 + \epsilon_2{}^2)^{1/2}$.

$$R = \frac{1 + |\epsilon| - [2(|\epsilon| + \epsilon_1)]^{1/2}}{1 + |\epsilon| + [2(|\epsilon| + \epsilon_1)]^{1/2}}$$

(44) (a) Tanner, D. R. ref. 2e, Vol. 2, pp 205–268. (b) Madison, M. R.; Coleman, L. B.; Somoano, R. B. *Solid State Commun.* **1981**, *40*, 979–982. (c) Weinstein, B. A.; Slade, M. L.; Epstein, A. J.; Miller, J. S. *Solid State Commun.* **1981**, *37*, 643–646, and references therein. (d) Torrance, J. B.; Scott, B. A.; Welber, B.; Kaufman, F. B.; Seiden, P. E. *Phys. Rev. B* **1979**, *19*, 730–741. (e) Delhaes, P.; Coulon, C.; Amiell, J.; Flandrois, S.; Toreilles, E.; Fabre, J. M.; Giral, L. *Mol. Cryst. Liq. Cryst.* **1979**, *50*, 43–58. (f) Jacobsen, C. S.; Mortensen, K.; Andersen, J. R.; Bechgaard, K. *Phys. Rev. B* **1978**, *18*, 905–921. (g) Somoano, R. B.; Yen, S. P. S.; Hadek, V.; Khanna, S. K.; Novotny, M.; Datta, T.; Hermann, A. M.; Woollam, J. A. *Phys. Rev. B* **1978**, *17*, 2853–2857.

(45) Almeida, M.; Tonge, L. S.; Inabe, T.; Kannewurf, C. R.; Marks, T. J., manuscript in preparation.

Table V. Room Temperature (300 K) Four-Probe Electrical Conductivity Data for Polycrystalline $\{[Si(Pc)O]X_y\}_n$ Samples

compound	σ (300 K), Ω^{-1} cm^{-1}
$[Si(Pc)O]_n$	5.5×10^{-6} [a]
$\{[Si(Pc)O](I_3)_{0.37}\}_n$	5.8×10^{-1} [a]
$\{[Si(Pc)O](BF_4)_{0.11}\}_n$	3.7×10^{-3}
$\{[Si(Pc)O](BF_4)_{0.18}\}_n$	2.4×10^{-2}
$\{[Si(Pc)O](BF_4)_{0.20}\}_n$	5.3×10^{-2}
$\{[Si(Pc)O](BF_4)_{0.28}\}_n$	6.7×10^{-2}
$\{[Si(Pc)O](BF_4)_{0.31}\}_n$	9.0×10^{-2}
$\{[Si(Pc)O](BF_4)_{0.36}\}_n$	8.6×10^{-2}
$\{[Si(Pc)O](PF_6)_{0.08}\}_n$	1.3×10^{-2}
$\{[Si(Pc)O](PF_6)_{0.18}\}_n$	1.7×10^{-2}
$\{[Si(Pc)O](PF_6)_{0.20}\}_n$	2.3×10^{-2}
$\{[Si(Pc)O](PF_6)_{0.32}\}_n$	7.8×10^{-2}
$\{[Si(Pc)O](SbF_6)_{0.39}\}_n$	1.5×10^{-1}

[a] Reference 7c.

partially oxidized phthalocyanine materials are compiled in Table IV. The data for the four $[Si(Pc^{\rho+})O]_n$ materials are identical within experimental error. Differences observed for $\{[Ge(Pc)O](I_3)_{0.37}\}_n$ and $Ni(Pc)(I_3)_{0.33}$ are logically explained in terms of the differing Pc–Pc interplanar spacings and other structural features.[7c]

$\{[Si(Pc)O]X_y\}_n$ Charge Transport Properties. Four-probe electrical conductivity measurements were performed on the same type of pressed sample pellets as were employed for the X-ray diffraction and optical reflectance studies. Instrumentation and precautions were the same as described previously.[7c] It is expected that conductivity results on polycrystalline samples of low-dimensional conductors are influenced by the intrinsic isotropy of the measurement technique and by the effects of interparticle contact resistance. While measurements on high-quality single crystals would obviously be more desirable (although not without their own problems and ambiguities[46-48]), such sample types are not available for any series of doped conductive polymers, and polycrystalline conductivity data can still be highly informative.[7c] This should be especially true for a chemically related series of materials having the same chemical precursor, similar chemical compositions, similar crystal structures, and in which crystallite orientation information is in hand. A great deal of empirical information indicates that the dc conductivities of low-dimensional molecular "metals" are typically 10^2–10^3 greater when measured on single crystal specimens in the molecular stacking direction than when measured on compressed polycrystalline samples.[7c,24,49] The temperature dependence of the conductivity is also different for single crystals and polycrystalline compactions; however, the nature of the differences is qualitatively predictable,[7c] and techniques exist (e.g., voltage-shorted compaction[7c,50]) which reveal aspects of single-crystal behavior even in polycrystalline samples. In regard to phthalocyanine materials, we have found the above single crystal–polycrystalline generalizations to hold well for

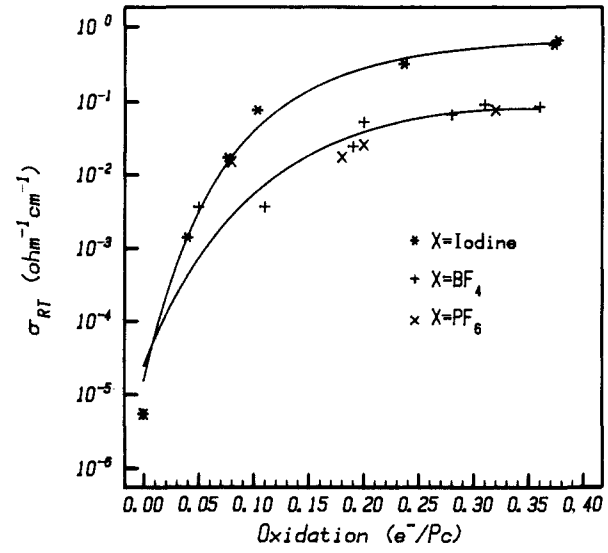

Figure 13. Electrical conductivity at 300 K for polycrystalline $\{[Si(Pc)O]X\}_n$ samples as a function of the average degree of oxidation per Si(Pc) unit. Lines connecting the points are drawn as guides to the eye.

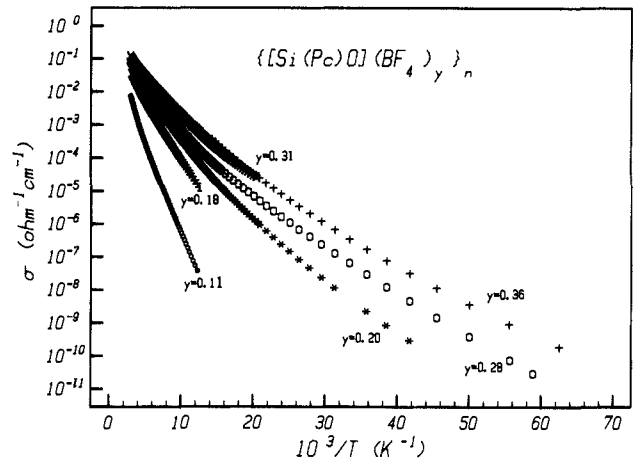

Figure 14. Variable temperature electrical conductivity data for polycrystalline $\{[Si(Pc)O](BF_4)_y\}_n$ samples at various doping levels.

$Ni(Pc)(I_3)_{0.33}$,[7c] $H_2(Pc)(I_3)_{0.33}$,[24] and $Ni(Pc)(BF_4)_{0.35}$.[30] Thus, it should be possible to make reasonable extrapolations from polycrystalline $\{[Si(Pc)O]X_y\}_n$ conductivity data to anisotropic charge transport behavior in the polymer chain direction.

Room temperature conductivity data for various polycrystalline $\{[Si(Pc)I]X_y\}_n$ materials are set out in Table V. That these results are not significantly influenced by preferential crystallite orientation was demonstrated by using techniques described previously.[7c] Room temperature conductivity data as a function of the average degree of partial oxidation per Si(Pc) unit are shown in Figure 13. At all doping levels, it can be seen that polycrystalline conductivities of the various $\{[Si(Pc)O]X_y\}_n$ materials are similar. This agrees with the optical conductivity results of the previous section (Table IV). By using the aforementioned polycrystalline → single crystal rule of thumb, it can be anticipated that the dc conductivity in the $[Si(Pc^{\rho+})O]_n$ chain direction will be ca. 50–100 Ω^{-1} cm^{-1} for these materials. Small differences between the various compounds more likely reflect surface chemical effects and interparticle contact resistance differences than anything related to the band structure.

It can be seen in Figure 13 that the functional dependence of σ and ρ is rather similar for the $X^- = BF_4^-$, PF_6^-, and I_3^- polymers (insufficient $X^- = SbF_6^-$ data were available for a similar treatment). In the case of incremental iodine doping, it was noted[7c] that the behavior consisting of a relatively abrupt increase in conductivity followed by a levelling-off at relatively low doping levels was reminiscent of three-dimensional percolation phenomena.[16c,51,52] For a randomly dispersed (inhomogeneous) mixture

(46) (a) Single crystal conductivity data can be strongly influenced by strain, disorder, defects, impurities, and other factors related to the starting materials and the crystallization process.[24,46b-e] Moreover, even in cases of optimum contact alignment,[47] other measurement-dependent phenomena such as contact strain[48a] and cooling rate effects[48a,b] can have major consequences for the observed temperature dependence of the conductivity. (b) Khanna, S. K.; Wuller, W. W.; Grüner, G.; Chaikin, P. M. *Phys. Rev. B* **1981**, *24*, 2958–2963, and references therein. (c) Heeger, A. J. In *Highly Conducting One-Dimensional Solids*; Devrees, J. T., Evrard, R. P., van Doren, V. W., Eds.; Plenum Press: New York, 1979; pp 105–120. (d) Begg, I. D.; Roberts, K. J.; Sherwood, J. N.; Groth-Andersen, L.; Jacobsen, C. S. *Chem. Phys. Lett.* **1981**, *79*, 513–516. (e) Parkin, S. S.; Creuzet, F.; Jérome, D.; Fabre, J. M.; Bechgaard, K. *J. Phys.* **1983**, *44*, 975–984.

(47) Shafer, D. E.; Wudl, F.; Thomas, G. A.; Ferraris, J. P.; Cowan, D. O. *Solid State Commun.* **1974**, *14*, 347–352.

(48) (a) Inabe, T.; Lyding, J. W.; Kannewurf, C. R.; Marks, T. J., unpublished results. (b) Kagoshima, S.; Yasunaga, T.; Ishiguro, T.; Anzai, H.; Saito, G. *Solid State Commun.* **1983**, *46*, 867–870, and references therein.

(49) (a) Chiang, C. K.; Druy, M. A.; Gau, S. C.; Heeger, A. J.; Louis, E. J.; MacDiarmid, A. G. *J. Am. Chem. Soc.* **1978**, *100*, 1013–1015. (b) Chiang, C. K.; Park, Y. W.; Heeger, A. J.; Shirakawa, H.; Louis, E. J.; MacDiarmid, A. G. *J. Chem. Phys.* **1978**, *69*, 5098–5104. (c) Farges, J. P.; Brau, A.; Gutmann, F. *J. Phys. Chem. Solids* **1972**, *33*, 1723–1726.

(50) Coleman, L. B. *Rev. Sci. Instrum.* **1978**, *49*, 58–63.

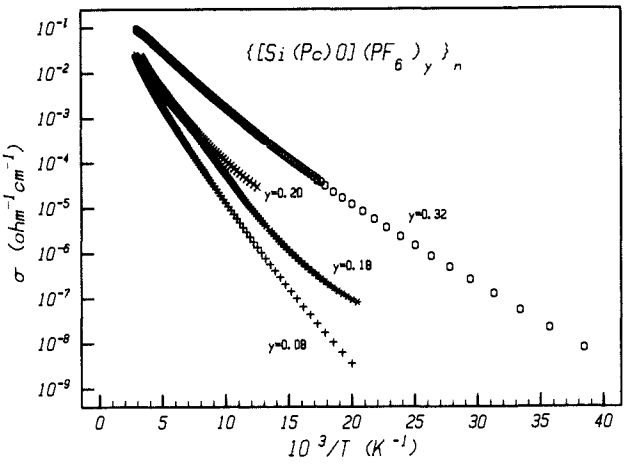

Figure 15. Variable temperature electrical conductivity data for polycrystalline $\{[Si(Pc)O](PF_6)_y\}_n$ samples at various doping levels.

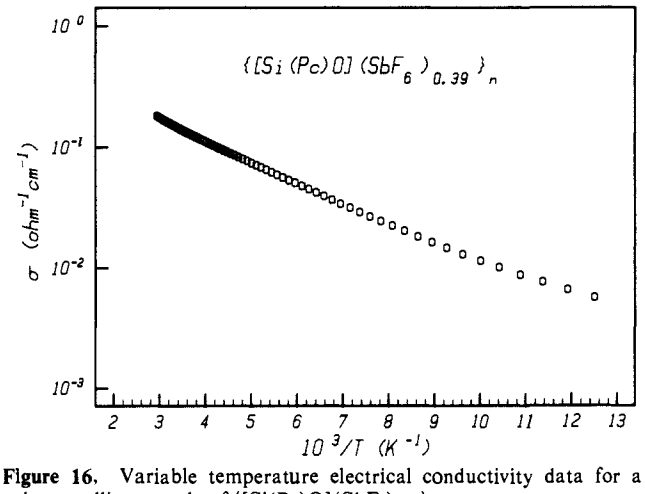

Figure 16. Variable temperature electrical conductivity data for a polycrystalline sample of $\{[Si(Pc)O](SbF_6)_{0.39}\}_n$.

of conductive and nonconductive particles having similar shapes and sizes, theory predicts adherence to eq 7 in the composition

$$\sigma = \sigma_0(X - X_c)^s \quad (7)$$

region near and above the insulator-to-conductor (percolation) threshold.[51] Here X is the volume fraction of conductive species, and X_c is the percolation threshold below which conductivity falls precipitously. For iodine doping of $[Si(Pc)O]_n$, it was found that the X_c and s parameters obtained from a fit to eq 7 ($X_c = 0.09$ (1), $s = 1.8$ (2)) were in agreement with those commonly observed in well-characterized three-dimensional percolation systems ($X_c \sim 0.15$, $s = 1.5$–1.7).[51-53] From Figure 13 it thus appears that a simple percolation model, consistent with the inhomogeneous nature of the doping process, qualitatively explains the charge transport characteristics as a function of doping level for all the $\{[Si(Pc)O]X_y\}_n$ materials.[53]

Variable temperature conductivity data for $\{[Si(Pc)O]X_y\}_n$ polymers are presented in a log σ vs. $1/T$ format in Figures 14–16. The general behavior is reminiscent of the $\{[Si(Pc)O](I_3)_y\}_n$ ma-

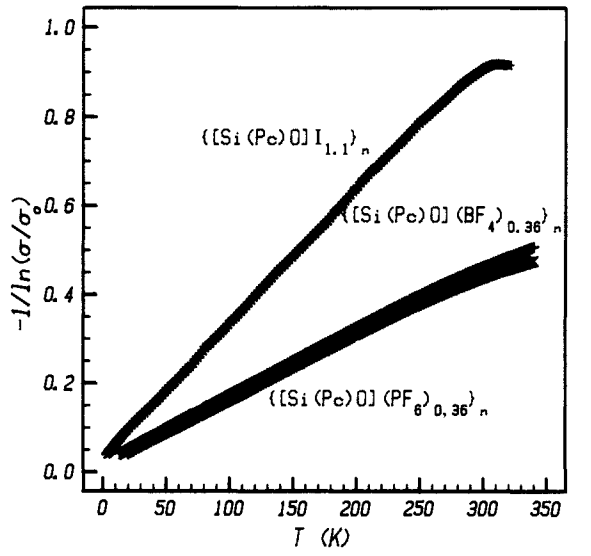

Figure 19. Conductivity data for polycrystalline doped polymer samples plotted in accordance with the fluctuation-induced tunneling model of eq 9.

Table VI. Fluctuation-Induced Tunneling Analysis Results for Polycrystalline $\{[Si(Pc)O]X_y\}_n$ Samples[a]

compound	σ_0, Ω^{-1} cm^{-1}	T_1, K	T_0, K
$\{[Si(Pc)O]I_{1.1}\}_n$	1.74 (3)	330 (3)	9.5 (3)
$\{[Si(Pc)O](BF_4)_{0.36}\}_n$	0.43 (5)	572 (5)	10.7 (3)
$\{[Si(Pc)O](PF_6)_{0.36}\}_n$	0.36 (5)	595 (5)	7.7 (3)

[a] Calculated from a least-squares fit to eq 9.

terials: decreasing slope with increasing doping level and a decrease in slope at lower temperatures.[7c] Similar behavior is observed for a number of other doped conductive polymer systems.[16] In the case of the $\{[Si(Pc)O](I_3)_y\}_n$ polymers, unsuccessful attempts were made to fit the data to eq 8, where $a = 0.50$ has been

$$\sigma = Ae^{-(T_0/T)^a} \quad (8)$$

associated with carrier tunneling between small metallic particles in an insulating matrix, one-dimensional carrier hopping between localized states, or certain types of disorder,[54,55] and where $a = 0.25$ has been associated with three-dimensional variable range carrier hopping between localized states.[56-58] Instead, the $\{[Si(Pc)O](I_3)_y\}_n$ data could be more satisfactorily fit to a fluctuation-induced tunneling model originally developed for (inhomogeneous) composite materials.[59] This description assumes relatively large conductive regions separated by insulating barriers having a parabolic potential. Conductivity displays thermally activated characteristics at higher temperatures but is dominated by temperature-independent elastic tunneling at low temperatures. The conductivity can be expressed as in eq 9 where the parameters T_1 and T_0 are given in eq 10 and 11. Here A is the barrier

(51) (a) Kirkpatrick, S. *Rev. Mod. Phys.* **1973**, *45*, 574–588, and references therein. (b) Seager, C. H.; Pike, G. E. *Phys. Rev. B* **1974**, *10*, 1435–1446, and references therein. (c) Hsu, W. Y.; Barkley, J. R.; Meakin, P. *Macromolecules* **1980**, *13*, 198–200. (d) Lagues, M.; Sauterey, C. *J. Phys. Chem.* **1980**, *84*, 3503–3508.

(52) (a) Clarke, P. S.; Orton, J. W.; Guest, A. J. *Phys. Rev. B* **1978**, *18*, 1813–1817, and data cited therein. (b) Malliaris, A.; Turner, D. T. *J. Appl. Phys.* **1971**, *42*, 614–618.

(53) In principle, a region in which σ is almost independent of doping level should be observable at very low y values (below the percolation threshold). For the present systems, the possibility that $[Si(Pc)O]_n$ has already been lightly doped by trace impurities (especially at the >400 °C polymerization temperature) and the experimental difficulty of accurately measuring y at very low y values has so far rendered meaningful studies in this doping regime impracticable.

(54) (a) Sheng, P. *Phys. Rev. Lett.* **1973**, *31*, 44–47. (b) Sichel, E. K.; Gittleman, J. I.; Sheng, P. *Phys. Rev. B* **1978**, *18*, 5712–5716. (c) Sichel, E. K. *Appl. Phys. Commun.* **1981**, *1*, 83–96. (d) Abeles, B.; Sheng, P.; Coutts, M. D.; Arie, Y. *Adv. Phys.* **1975**, *24*, 407–461.

(55) (a) Tomkiewicz, Y.; Shiren, N. S.; Schultz, T. D.; Thomann, H.; Dalton, L. R.; Zettl, A.; Grüner, G.; Clarke, T. C. *Mol. Cryst. Liq. Cryst.* **1982**, *83*, 17–31. (b) Mortensen, K.; Thewalt, M. L. W.; Tomkiewicz, Y.; Clarke, T. C.; Street, G. B. *Phys. Rev. Lett.* **1980**, *45*, 490–495. (c) Shacklett, L. W.; Chance, R. R.; Ivory, D. M.; Miller, G. G.; Baughman, R. H. *Synth. Met.* **1979**, *1*, 307–320.

(56) (a) Mott, N. F.; Davis, E. A. *Electronic Processes in Noncrystalline Materials*, 2nd ed.; Claredon: Oxford, 1979. (b) Mott, N. F. *Festkörperprobleme* **1979**, *XIX*, 331–361.

(57) Epstein, A. J.; Rommelmann, H.; Bigelow, R.; Gibson, H. W.; Hoffman, D. M.; Tanner, D. B. *J. Phys.* **1983**, *C3*, 61–68.

(58) Colson, R.; Nagles, P. *J. Non-Cryst. Solids* **1980**, *36*, 129–134, and references therein.

(59) (a) Sheng, P. *Phys. Rev. B* **1980**, *21*, 2180–2195. (b) Park, J.-W.; Heeger, A. J.; Druy, M. A.; MacDiarmid, A. G. *J. Chem. Phys.* **1980**, *73*, 946–957.

$$\sigma = \sigma_0 e^{-[T_1/(T+T_0)]} \quad (9)$$

$$T_1 = \frac{2AV_0^2}{\pi e^2 k W} \quad (10)$$

$$T_0 = \frac{4\hbar A V_0^{3/2}}{\pi^2 e^2 k W^2 (2m)^{1/2}} \quad (11)$$

cross-sectional area (in Å^2), V_0 is the barrier height, k is Boltzmann's constant, W is the barrier thickness (in Å), and m is the effective carrier mass. As can be seen in Figure 17 (see Supplementary Material),[60] the $\{[Si(Pc)O](BF_4)_{0.36}\}_n$ and $\{[Si(Pc)O](PF_6)_{0.36}\}_n$ data do not conform well to eq 8 for either $a = 0.50$ or $a = 0.25$ (the fit is somewhat better for the former which probably corresponds to a less likely process). It can be seen in Figure 18 (see Supplementary Material)[60] that another variable range hopping version of eq 8[57] where $A = T^{1/2}$ and $a = {}^1/_4$ is equally inappropriate. In contrast to these results, the fit to the fluctuation-induced tunneling model (eq 9) is more convincing (Figure 19), and deviations (as predicted[59a]) are only observed at higher temperatures where "metal-like" behavior is operative. Values of σ_0, T_1, and T_0 obtained by a least-squares fit of the data in Figure 19 to eq 9 are presented in Table VI. It is apparent that these barrier parameters are rather similar for $\{[Si(Pc)O](I_3)_{0.37}\}_n$, $\{[Si(Pc)O](BF_4)_{0.36}\}_n$, and $\{[Si(Pc)O](PF_6)_{0.36}\}_n$.

Discussion

Doping Chemistry and Thermodynamics. In regard to chemistry, perhaps the most intriguing result of this study is the observation that the maximum degree of partial oxidation (band filling) achieved in the doping process is, within experimental error, identical for Br_2, I_2, $NO^+BF_4^-$, $NO^+PF_6^-$, and $NO^+SbF_6^-$ as oxidants: $\rho \approx +0.36$. The reason why such seemingly disparate oxidizing agents should result in essentially the same degree of partial oxidation is not immediately obvious. Indeed, those factors which determine crystal packing patterns and electronic charge distribution in mixed-valent organic lattices are not, in general, well understood.[3a,4,9,61] However, the structural invariance of the $[Si(Pc)O]_n$ cofacial array both before and after doping is especially attractive for examining the energetic aspects of the problems.[62]

Two thermodynamic parameters are important in describing the energetics of forming a donor–acceptor lattice. For D = donor molecule, A = acceptor molecule, the enthalpy of mixing or charge transfer for the process in eq 12 is given by eq 13 where c refers to crystal. For a system with complete charge transfer ($\rho = 1$),

$$D_{(c)} + A_{(c)} \rightarrow D^{\rho+}A^{\rho-}{}_{(c)} \quad (12)$$

$$\Delta H_{ct} = \Delta H_f^\circ(DA)_{(c)} - \Delta H_f^\circ(D)_{(c)} - \Delta H_f^\circ(A)_{(c)} \quad (13)$$

the cohesive energy (the crystal binding energy) U is the energy describing the process in eq 14, which can be expressed via a Born–Haber cycle as in eq 15[4,61] where sub refers to sublimation,

$$D^+_{(g)} + A^-_{(g)} \rightarrow D^+A^-_{(c)} \quad (14)$$

$$\begin{aligned} U(DA) &= \Delta H_f^\circ(DA)_{(c)} - \Delta H_f^\circ(D^+)_{(g)} - \Delta H_f^\circ(A^-)_{(g)} + 2RT \\ &= \Delta H_f^\circ(DA)_{(c)} - \Delta H_f^\circ(D)_{(c)} - \Delta H_f^\circ(A)_{(c)} - \Delta H^\circ{}_{sub}(D) - \\ &\quad \Delta H^\circ{}_{sub}(A) - IP(D) + EA(A) + 2RT \end{aligned} \quad (15)$$

IP to gas phase adiabatic ionization potential, and EA to gas phase adiabatic electron affinity. Appropriate modifications can be made for cases of nonintegral charge transfer ($\rho \neq 1$).[4,61] In regard to contributing terms, U has usually been expressed as in eq 16[4d]

$$\begin{aligned} -U \approx \rho[IP(D) - EA(A)] + \rho^2 E_M + \rho^2 E_{ex} + \rho^2 E_{pol} + E_B^\rho + \\ E_{vdW}^\rho + E_{CR}^\rho \end{aligned} \quad (16)$$

where E_M is the Madelung energy, E_{ex} is the exchange energy, E_{pol} is the polarization energy gained by interaction with dipoles induced on neighboring sites, E_B^ρ is the energy gained by band formation, E_{vdW}^ρ is the van der Waals energy, and E_{CR}^ρ is the core repulsion energy.

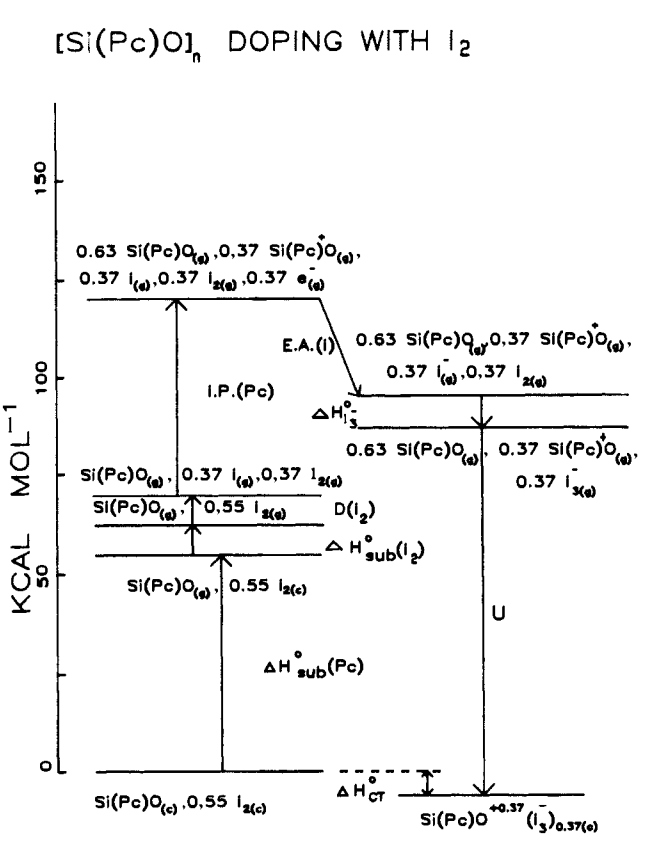

Figure 20. Born–Haber cycle for the doping of "Si(Pc)O" with iodine to "$[Si(Pc)O]I_{1.1}$". The parameters in Table VII were employed and modified for the reaction stoichiometry where appropriate.

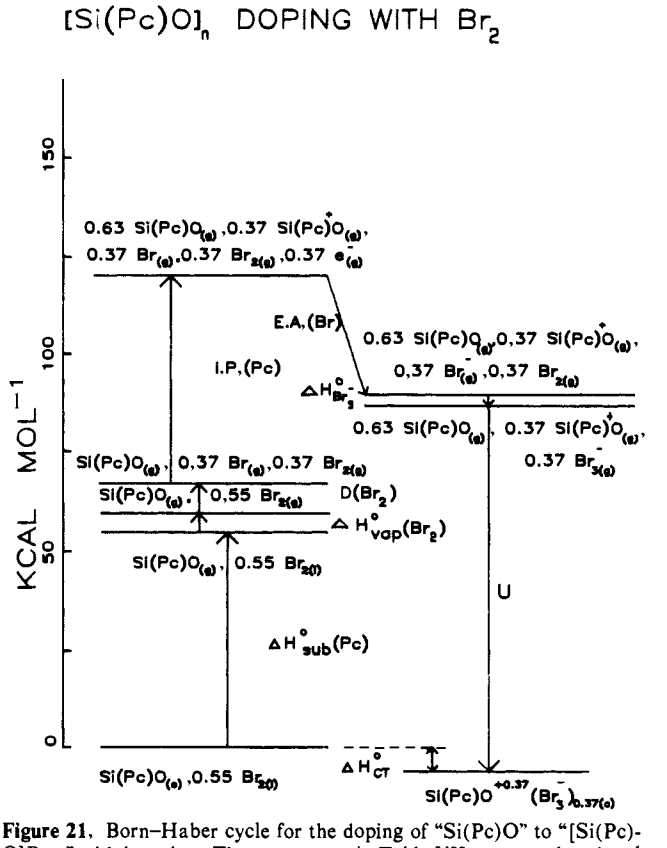

Figure 21. Born–Haber cycle for the doping of "Si(Pc)O" to "$[Si(Pc)O]Br_{1.1}$" with bromine. The parameters in Table VII were employed and modified for the reaction stoichiometry where appropriate.

(60) See paragraph at end of paper regarding supplementary material.
(61) (a) Metzger, R. M. *J. Chem. Phys.* **1977**, *66*, 2525–2533. (b) Metzger, R. M.; Arafat, E. S. *J. Chem. Phys.* **1983**, *78*, 2696–2705. (c) Metzger, R. M.; Arafat, E. S.; Kuo, C. S. *J. Chem. Phys.* **1983**, *78*, 2706–2709.
(62) Pietro, W. J.; Marks, T. J., submitted for publication.

Table VII. Parameters in Born–Haber Cycles for $[Si(Pc)O]_n$ Doping and Sources[i]

	1. Phthalocyanines
$\Delta H°_{sub}(Pc)$	$= +56.7$[a]
IP(PC)	$= +147.6$[b]
	2. $[Si(Pc)O]_n + I_2$
$\Delta H°_{sub}(I_2)$	$= +14.9$[c]
$D(I_2)$	$= 36.1$[c]
EA(I)	$= +70.6$[d]
$\Delta H(I_3^-)$	$= -24$[c]
$\Delta H°_{CT}$	$= -2.9$[e]
	3. $[Si(Pc)O]_n + Br_2$
$\Delta H_{vap}(Br_2)$	$= +7.1$[c]
$D(Br_2)$	$= +46.1$[c]
EA(Br)	$= +79.0$[d]
$\Delta H(Br_3^-)$	$= -14$[f]
$\Delta H°_{CT}$	$= -4.9$[e]
	4. $[Si(Pc)O]_n + NO^+ClO_4^-$
$U(NO^+ClO_4^-)$	$= \Delta H_f°(NO^+ClO_4^-)(c) + 2RT - H_f°(NO^+)(g) - \Delta H_f°(ClO_4^-)(g)$
	$= -138.1$[g]
$EA(NO^+)$	$= +213.3$[h]

[a] Reference 63. [b] References 22 and 64. [c] Reference 68. [d] Reference 69. [e] Reference 62. [f] Estimated from the data of ref 68 as described in the text. [g] Reference 72. [h] Reference 73. [i] Given in kcal mol^{-1}.

For the systems $[Si(Pc)O]_n + I_2$ or Br_2, all data are available to construct Born–Haber cycles and to determine U. The results are shown in Figures 20 and 21. The parameters employed in these cycles are compiled in Table VII. For $\Delta H°_{sub}(Pc)$, $[Si(Pc)O]_n$ is treated as a molecular phthalocyanine, and the enthalpy of sublimation value for Ni(Pc)[63] is employed (any error in this term will be a constant in all of our calculations). For IP(Pc), we employ our PES(adiabatic) value[22] for $Si(Pc)(OR)_2$, R = $Si[C(CH_3)_3](CH_3)_2$. PES derived values for other M(Pc) molecules are essentially identical;[64] however, electron-impact-derived IP values[65] have been known[64a] to be incorrect (by greater than 22 kcal mol^{-1}) for some time and introduce a serious error in the calculations. For the $I_{2(g)} + I^-_{(g)} \rightarrow I_3^-{}_{(g)}$ enthalpy, we take the experimental, thermochemical value.[66] The value derived by Hückel calculations[67] is incorrect by greater than 25 kcal mol^{-1} and also introduces serious error in the calculations. Similar ΔH data are not available for Br_3^-; however, it is possible to estimate a reasonable value from the Br/I proportionality in formation constants for the $X_2 + X^- = X_3^-$ equilibrium in nonpolar solvents.[68] Other parameters for the halogen atoms and molecules are taken from standard sources.[68,69] We report the measurement of $\Delta H°_{CT}$ for these systems elsewhere.[62] Examination of the data in Table VII as well as Figures 20 and 21 reveals that the Born–Haber cycles are very similar and within experimental error, the cohesive energies of $\{[Si(Pc)O](I_3)_{0.37}\}_n$ and $\{[Si(Pc)O](Br_3)_{0.37}\}_n$ are virtually identical at −94 and −96 kcal mol^{-1}, respectively. The reason for the similarities in I_2/Br_2 cycles reflects near cancellations in many of the terms. Thus, while I_2 requires greater energy to volatilize, the bond dissociation energy is smaller; while the electron affinity of I is less negative, the formation enthalpy of the corresponding trihalide ($\Delta H°_{X_3^-}$) is more negative. The rather small magnitudes of $\Delta H°_{CT}$ are typical of low-dimensional mixed-valent organic conductors[4,61,62,70,71] and, in the present case, suggest that the energies involved in reorganizing donor lattices into cofacial D_n stacks are probably rather small.

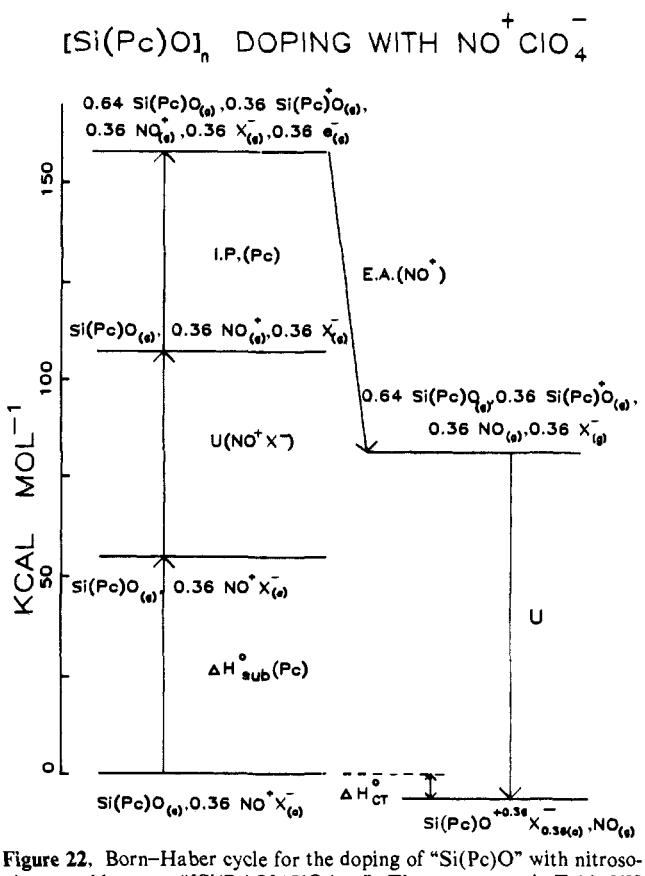

Figure 22. Born–Haber cycle for the doping of "Si(Pc)O" with nitrosonium perchlorate to "$[Si(Pc)O](ClO_4)_{0.36}$". The parameters in Table VII were employed and modified for the reaction stoichiometry where appropriate.

In examining the $NO^+BF_4^-$, $NO^+PF_6^-$, and $NO^+SbF_6^-$ doping thermodynamics, use was necessarily made of the only available thermodynamic data for a similar nitrosonium salt, $NO^+ClO_4^-$.[72] The data employed are given in Table VII, and the resulting Born–Haber cycle is shown in Figure 22. Interestingly, while the energy required to vaporize $NO^+ClO_4^-$ is greater than for the halogens, it is largely offset by the very large electron affinity of NO^+. The result is that $U - \Delta H°_{CT}$ for $\{[Si(Pc)O](ClO_4)_{0.36}\}_n$ is estimated to be −84 kcal mol^{-1}, surprisingly close to calculated values of −91 kcal mol^{-1} for $\{[Si(Pc)O](I_3)_{0.37}\}_n$ and −91 kcal mol^{-1} for $\{[Si(Pc)O](Br_3)_{0.37}\}_n$. Although $\Delta H°_{CT}$ has not been measured for any of the $\{[Si(Pc)O]X_{0.36}\}_n$, X = BF_4^-, PF_6^-, and SbF_6^- salts, it is likely to be small judging from the aforementioned literature $\Delta H°_{CT}$ values for other systems. With specific reference to $[Si(Pc)O]_n$ and other oxidants, $\Delta H°$ for $\{[Si(Pc)O](TCNQ)_x\}_n$ is found to be −3.3 kcal mol^{-1} [71]—again rather close to the values given above for I_2 and Br_2 (vide supra).

While this discussion does not explain exactly "why" the degree of $[Si(Pc)O]_n$ partial oxidation is so similar for seemingly diverse oxidants, it does reveal that the cohesive energies of the *observed* products are surprisingly similar. Although X_3^- filling of the counterion channels (Figure 6) might be invoked to rationalize the limiting $\rho \approx 0.35$ values for halogens, the structural data for

(63) MacKay, A. G. *Austr. J. Chem.* **1973**, *26*, 2425–2433.
(64) (a) Berkowitz, J. *J. Chem. Phys.* **1979**, *70*, 2819–2828. (b) Ciliberto, E.; Fragalà, I.; Marks, T. J., manuscript in preparation.
(65) Eley, E. E.; Hazeldine, D.; Palmer, T. J. *J. Chem. Soc., Faraday Trans. 2* **1973**, *69*, 1808–1814.
(66) Topol. L. E. *Inorg. Chem.* **1971**, *10*, 736–740.
(67) Wiebenga, E. H.; Kracht, D. *Inrog. Chem.* **1969**, *8*, 738–746.
(68) Downs, A. J.; Adams, C. J. In *Comprehensive Inorganic Chemistry*; Bailar, J. C., Emeléus, H. J., Nyholm, R., Trotman-Dickenson, A. F., Eds.; Pergamon Press: Oxford, 1973; Vol. 2, pp 1109, 1162–1163, 1173–1174, 1543.
(69) Hotop, H.; Lineberger, W. C. *J. Phys. Chem. Ref. Data* **1975**, *4*, 539–576.
(70) (a) Gutmann, F.; Hermann, A. M.; Rembaum, A. *J. Electrochem. Soc.* **1967**, *114*, 323–329. (b) Aronson, S.; Sinensky, G.; Langsam, Y.; Binder, M. *J. Inorg. Nucl. Chem.* **1976**, *38*, 407–410. (c) McKechnie, J. S.; Turner, L. D. S.; Vincent, C. A. *J. Chem. Thermodyn.* **1979**, *11*, 1189–1195. (d) Aronson, S.; Mittelman, J. S. *J. Solid State Chem.* **1981**, *36*, 221–224. (e) Matsumoto, T.; Matsunaga, Y. *Bull. Chem. Soc. Jpn.* **1981**, *54*, 648–653. (f) Euler, W. B.; Melton, M. E.; Hoffman, B. M. *J. Am. Chem. Soc.* **1982**, *104*, 5966–5971.
(71) Pietro, W. J.; Marks, T. J., manuscript in preparation.
(72) (a) Finch, A.; Gates, P. N.; Page, T. H. *J. Inorg. Nucle. Chem.* **1980**, *42*, 292–293. (b) Finch, A.; Gates, P. N.; Page, T. H. *J. Chem. Soc., Dalton Trans.* **1980**, 2415–2417.

the present systems reveal that small counterions such as BF_4^- leave ample space for additional charge compensators. Indeed, in results to be discussed elsewhere,[17] it is demonstrated that y for $\{[Si(Pc)O](BF_4)_y\}_n$ can be displaced as far as 0.50 by using electrochemical techniques at rather high voltages and that $\rho > +0.35$ values can be achieved with very strong organic oxidizing agents.[74] Nevertheless, the region of $\rho \approx +0.35$, which is a value somewhat less than is usually observed for molecular metals,[2-9] has considerable stability for these phthalocyanine systems.

Band Structure–Counterion Interactions. Another striking observation of the present study is the marked insensitivity of the $[Si(Pc^{\rho+})O]_n$ core to the identity of the off-axis counterions. This is seen not only in the stoichiometries achieved (ρ, vide supra) but also in architecture. While the cofacial nature of the phthalocyanine stacking is essentially fixed, the staggering angle between neighboring rings is not. Nevertheless, the observed angle of ca. 40° is, within experimental error, insensitive to counterion and in fact appears to be ubiquitous for partially oxidized phthalocyanines.[3a,7,24,29,30] It is observed for several integral oxidation states as well as cofacially stacked phthalocyanines.[7d,22,75] As pointed out by several groups,[22,76,77] this conformation approaches one of the two maxima (ϕ = 0° and 45°) in PC HOMO–HOMO overlap. Also of note and in accord with observations regarding halogen doping,[7d] the Si(Pc)–Si(Pc) interplanar spacing undergoes a small but perceptible contraction upon oxidation. This is in accord with the antibonding or nonbonding character of the band energy levels[22,76,77] being depleted.

The insensitivity of $\{[Si(Pc)O]X_y\}_n$ collective properties to the identity of X^-, where X^- varies from large, polarizable, elongated I_3^- to small, hard, spherical BF_4^-, stands in contrast to results for many low-dimensional molecular conductors.[2] For example, assuming that Coulomb repulsion between carriers is responsible for the small values of the magnetically-derived bandwidths (i.e., Coulomb-enhancement of the susceptibilities, Tables III and IV), then the constance of susceptibility as a function of X^- argues that counterion screening[3b,5b,41] must be small (or inexplicably constant). Likewise, the insensitivity of the plasma frequency to X^- (Table IV) argues, in agreement with the metrical parameters (Table II), that the band structure is not strongly coupled to the off-axis counterions. The room temperature conductivity is slightly more sensitive to X^- (Table V), but the differences are small considering the limitations of pressed pellet measurements. The temperature dependencies of the charge transport, as expressed by fluctuation-induced tunneling parameters (Table VI), are also similar for different X^- ions. The same is true for optically derived dc conductivities (Table IV).

Two features appear to be responsible for the observed decoupling of the radical–cation band structure from the surrounding lattice. The first concerns the electronic and molecular structure of the phthalocyanine subunit. As noted elsewhere,[22,76,77] the conduction band is constructed from phthalocyanine highest occupied molecular orbitals (HOMO's) which are localized, to a significant degree, toward the interior of the macrocycle.[76a] Combined with the steric constraints imposed upon approaching anions by the phalanx of benzo hydrogen atoms in the M(Pc) plane (Figure 6), the result is a minimization of the interaction that can take place between the M(Pc) π electrons and the X^- counterions. Such a situation is markedly different from that for many organochalcogen conductors[2,3,6] where HOMO-centered chalcogen-X interactions are, judging from metrical parameters and physical data, very strong.

The second feature of the $\{[Si(Pc)O]X_y\}_n$ systems which likely decreases the X^- influence on collective properties is the stacking rigidity imposed by the connectivity of the $(-Si-O-)_n$ chains. Thus, while the subunit packing in the crystal structures of many low-dimensional conductors, hence numerous collective properties, are highly sensitive functions of the size, polarizability, and other characteristics of lattice counterions,[2,3,6] deformations possible for the $[Si(Pc^{\rho+})O]_n$ lattice are far more restricted. In addition to static aspects it is likely that the collective properties of molecular conductors are strongly modulated by dynamic processes (electron–phonon).[42,77,78] Rigidly constraining the subunit stacking is likely to have a significant effect on certain motions (e.g., ring–ring stretching parallel to the stacking axis[55,78a]), hence on the temperature dependence of many carrier-related properties.

Cofacial assembly provides a unique means to study the properties of molecular conductors while holding essential structural characteristics constant or varying them in a controlled manner. In addition to interplanar spacing effects,[7c] the present work demonstrates that band structure–counterion interactions can be probed in such systems. We show elsewhere that the cofacially assembled architecture also allows an unprecedented tunability in band-filling for a molecular metal.[17]

Acknowledgment. This research was supported by the NSF-MFL program through the Materials Research Center of Northwestern University (Grant DMR 82-16972) and by the Office of Naval Research. J.W.L. thanks IBM Corporation for a postdoctoral fellowship.

Registry No. $[Ge(Pc)O]_n$, 55948-70-4; $[Si(Pc)O]_n$, 39114-20-0; $NO^+BF_4^-$, 14635-75-7; $NO^+PF_6^-$, 16921-91-8; $NO^+SbF_6^-$, 16941-06-3.

Supplementary Material Available: Figures 17 and 18, attempted fits for $\{[Si(Pc)O](BF_4)_{0.36}\}_n$ and $\{[Si(Pc)O](PF_6)_{0.36}\}_n$ variable temperature conductivity data to different hopping transport models (3 pages). Ordering information is given on any current masthead page.

(73) (a) Jones, K. ref 68, Vol. 2, p 327. (b) *JANAF Thermochemical Tables*, 2nd ed.; Natl. Stand. Ref. Data Ser.; 1971.
(74) (a) Moguel, M. K.; Marks, T. J., manuscript in preparation. (b) Moguel, M. K.; Marks, T. J. Abstracts of Papers, 190th National Meeting of the American Chemical Society, Chicago, IL; American Chemical Society: Washington, DC, Sept. 1985; INOR 138.
(75) Mossoyan-Deneux, M.; Benlian, D.; Ley, M.; Pierrot, M.; Sorbier, J. C.; Fournel, A. ref 2a, Vol. 120, pp 437–440.
(76) (a) Pietro, W. J.; Ratner, M. A.; Marks, T. J. *J. Am. Chem. Soc.* **1985**, *107*, 5387–5391. (b) Pietro, W. J.; Ellis, D. E.; Marks, T. J.; Ratner, M. A. *Mol. Cryst. Liq. Cryst.* **1984**, *105*, 273–287.
(77) (a) Whangbo,M.-H.; Stewart, K. R. *Isr. J. Chem.* **1983**, *23*, 133–138. (b) Canadell, E.; Alvarez, S. *Inorg. Chem.* **1984**, *23*, 573–579. (c) Böhm, M. C. *Chem. Phys.* **1984**, *86*, 17–30.
(78) (a) Hale, P. D.; Ratner, M. A. *J. Chem. Phys.* **1985**, *83*, 5277–5285. (b) Conwell, E. M. *Phys. Rev. B* **1980**, *22*, 1761–1780.